Oklahoma Department of Transportation
200 NE 21st Street, Oklahoma City, OK 73105-3204

FINAL REPORT ~ FHWA-OK-19-05

LONG TERM PAVEMENT PERFORMANCE MONITORING OF SIX LTPP SPS-10 SECTIONS IN OKLAHOMA WITH 3D LASER IMAGING

Kelvin C. P. Wang, Ph.D., P.E.
Joshua Q. Li, Ph.D. P.E.
Gary Guangwei Yang, Ph.D.

School of Civil and Environmental Engineering
College of Engineering, Architecture and Technology
Oklahoma State University
Stillwater, Oklahoma

December 2019

OKLAHOMA
Transportation

The Oklahoma Department of Transportation (ODOT) ensures that no person or groups of persons shall, on the grounds of race, color, sex, religion, national origin, age, disability, retaliation or genetic information, be excluded from participation in, be denied the benefits of, or be otherwise subjected to discrimination under any and all programs, services, or activities administered by ODOT, its recipients, sub-recipients, and contractors. To request an accommodation please contact the ADA Coordinator at 405-521-4140 or the Oklahoma Relay Service at 1-800-722-0353. If you have any ADA or Title VI questions email ODOT-ada-titlevi@odot.org.

LONG TERM PAVEMENT PERFORMANCE MONITORING OF SIX LTPP SPS-10 SECTIONS IN OKLAHOMA WITH 3D LASER IMAGING

FINAL REPORT ~ FHWA-OK-19-05

ODOT SP&R ITEM NUMBER 2115

Submitted to:

Office of Research and Implementation

Oklahoma Department of Transportation

Submitted by:

Kelvin Wang, Ph.D., P.E

Joshua Q. Li, Ph.D. P.E.

Gary Guangwei Yang, Ph.D.

Oklahoma State University

December 2019

TECHNICAL REPORT DOCUMENTATION PAGE

<table>
<tr><td colspan="2">1. REPORT NO.
FHWA-OK-19-05</td><td>2. GOVERNMENT ACCESSION NO.</td><td>3. RECIPIENT'S CATALOG NO.</td></tr>
<tr><td colspan="3">4. TITLE AND SUBTITLE
LONG TERM PAVEMENT PERFORMANCE MONITORING OF SIX LTPP SPS-10 SECTIONS IN OKLAHOMA WITH 3D LASER IMAGING</td><td>5. REPORT DATE
Dec 2019</td></tr>
<tr><td colspan="3" rowspan="2"></td><td>6. PERFORMING ORGANIZATION CODE</td></tr>
<tr><td colspan="3">7. AUTHOR(S)
Kelvin Wang, Ph.D., P.E. and Joshua Q. Li, Ph.D., P.E.</td><td>8. PERFORMING ORGANIZATION REPORT</td></tr>
<tr><td colspan="3">9. PERFORMING ORGANIZATION NAME AND ADDRESS

Oklahoma State University, Stillwater Oklahoma 74078</td><td>10. WORK UNIT NO.

11. CONTRACT OR GRANT NO.
ODOT SPR Item Number 2115</td></tr>
<tr><td colspan="3">12. SPONSORING AGENCY NAME AND ADDRESS

Oklahoma Department of Transportation
Office of Research and Implementation
200 N.E. 21st Street, Room G18
Oklahoma City, OK 73105</td><td>13. TYPE OF REPORT AND PERIOD COVERED
Final Report
Oct 2015 – Oct 2019

14. SPONSORING AGENCY CODE</td></tr>
<tr><td colspan="4">15. SUPPLEMENTARY NOTES
N/A</td></tr>
<tr><td colspan="4">16. ABSTRACT
Under the LTPP Specific Pavement Study 10 (SPS-10) experiment initiative, the Oklahoma Department of Transportation (ODOT) constructed five warm mix asphalt (WMA) testing sections and one hot mix asphalt (HMA) control section. In this project several art-of-the-state instruments were used to collect a comprehensive array of pavement surface characteristics data. The data collection was performed biannually for five years for long term field performance evaluation. It is demonstrated that four of the five WMA sites exhibit comparable performance as compared to that of the HMA section, in terms of pavement cracking, rutting, and roughness. In addition, aggregate properties and mixture design show impacts on pavement macrotexture and skid resistance properties.</td></tr>
<tr><td colspan="2">17. KEY WORDS
WMA, HMA, 3D Imaging, Cracking, Rutting, IRI, Texture, Skid Resistance</td><td colspan="2">18. DISTRIBUTION STATEMENT
No restrictions. This publication is available from the Office of Research and Implementation, Oklahoma DOT.</td></tr>
<tr><td>19. SECURITY CLASSIF. (OF THIS REPORT)
Unclassified</td><td>20. SECURITY CLASSIF. (OF THIS PAGE)
Unclassified</td><td>21. NO. OF PAGES
95</td><td>22. PRICE
N/A</td></tr>
</table>

Form DOT F 1700.7 (08/72)

SI* (MODERN METRIC) CONVERSION FACTORS

APPROXIMATE CONVERSIONS TO SI UNITS

SYMBOL	WHEN YOU KNOW	MULTIPLY BY	TO FIND	SYMBOL
		LENGTH		
in	inches	25.4	millimeters	mm
ft	feet	0.305	meters	m
yd	yards	0.914	meters	m
mi	miles	1.61	kilometers	km
		AREA		
in^2	square inches	645.2	square millimeters	mm^2
ft^2	square feet	0.093	square meters	m^2
yd^2	square yard	0.836	square meters	m^2
ac	acres	0.405	hectares	ha
mi^2	square miles	2.59	square kilometers	km^2
		VOLUME		
fl oz	fluid ounces	29.57	milliliters	mL
gal	gallons	3.785	liters	L
ft^3	cubic feet	0.028	cubic meters	m^3
yd^3	cubic yards	0.765	cubic meters	m^3
		NOTE: volumes greater than 1000 L shall be shown in m^3		
		MASS		
oz	ounces	28.35	grams	g
lb	pounds	0.454	kilograms	kg
T	short tons (2000 lb)	0.907	megagrams (or "metric ton")	Mg (or "t")
		TEMPERATURE (exact degrees)		
°F	Fahrenheit	5 (F-32)/9 or (F-32)/1.8	Celsius	°C
		ILLUMINATION		
fc	foot-candles	10.76	lux	lx
fl	foot-Lamberts	3.426	$candela/m^2$	cd/m^2
		FORCE and PRESSURE or STRESS		
lbf	poundforce	4.45	newtons	N
lbf/in^2	poundforce per square inch	6.89	kilopascals	kPa

APPROXIMATE CONVERSIONS FROM SI UNITS

SYMBOL	WHEN YOU KNOW	MULTIPLY BY	TO FIND	SYMBOL
		LENGTH		
mm	millimeters	0.039	inches	in
m	meters	3.28	feet	ft
m	meters	1.09	yards	yd
km	kilometers	0.621	miles	mi
		AREA		
mm^2	square millimeters	0.0016	square inches	in^2
m^2	square meters	10.764	square feet	ft^2
m^2	square meters	1.195	square yards	yd^2
ha	hectares	2.47	acres	ac
km^2	square kilometers	0.386	square miles	mi^2
		VOLUME		
mL	milliliters	0.034	fluid ounces	fl oz
L	liters	0.264	gallons	gal
m^3	cubic meters	35.314	cubic feet	ft^3
m^3	cubic meters	1.307	cubic yards	yd^3
		MASS		
g	grams	0.035	ounces	oz
kg	kilograms	2.202	pounds	lb
Mg (or "t")	megagrams (or "metric ton")	1.103	short tons (2000 lb)	T
		TEMPERATURE (exact degrees)		
°C	Celsius	1.8C+32	Fahrenheit	°F
		ILLUMINATION		
lx	lux	0.0929	foot-candles	fc
cd/m^2	$candela/m^2$	0.2919	foot-Lamberts	fl
		FORCE and PRESSURE or STRESS		
N	newtons	0.225	poundforce	lbf
kPa	kilopascals	0.145	poundforce per square inch	lbf/in^2

*SI is the symbol for the International System of Units. Appropriate rounding should be made to comply with Section 4 of ASTM E380. (Revised March 2003)

TABLE OF CONTENTS

The contents of this report reflect the views of the author(s) who is responsible for the facts and the accuracy of the data presented herein. The contents do not necessarily reflect the views of the Oklahoma Department of Transportation or the Federal Highway Administration. This report does not constitute a standard, specification, or regulation. While trade names may be used in this report, it is not intended as an endorsement of any machine, contractor, process, or product.

LIST OF FIGURES

LIST OF TABLES

CHAPTER 1 INTRODUCTION

1.1 Background

The use of warm mix asphalt (WMA) technology, which is defined as an asphalt concrete paving material produced and placed at temperatures approximately 50 °F cooler than those used for hot mix asphalt (HMA), offers significant benefits, notably, lower energy demand during production and construction, reduced emissions at the plant and the paver, and increased allowable haul distances (Button et al., 2007; D'Angelo et al., 2008; Bonaquist, 2011). As a result, WMA for asphalt pavement construction has dramatically increased in the United States over the past decade. At least 30 state departments of transportation (DOTs) have established specification permitting the use of WMA. Dozens of studies have been conducted to evaluate the performance of plant-produced lab-compacted mixtures utilizing various WMA technologies (Hurley et al., 2006; Diefenderfer and Hearon, 2008; D'Angelo et al., 2008; Bonaquist, 2011; Bower et al., 2012; Mohammad et al., 2014). Laboratory tests for WMA performance evaluation include dynamic modulus (E*), flow number (FN), loaded wheel tracking (LWT) test, indirect tensile (IDT) test, semicircular bend (SCB) test, thermal stress restrained specimen test (TSRST), and the Lottman moisture susceptibility test.

However, as WMA moves into mainstream use, one primary obstacle of WMA implementation is the uncertainty about how WMA may affect short- and long-term field performance (Prowell et al., 2007; Wielinski et al., 2009; Kvasnak et al., 2010;

Copeland et al., 2013; West et al., 2014). Lower WMA production temperatures and the water injection used with some WMA technologies have raised concerns on possible rutting and moisture susceptibility of WMA pavements. Several studies indicate the dis-connectivity between laboratory study results and field performance. WMA plant-produced samples have been compacted in the laboratory to simulate the actual aging that occurs in the field, but most of these mixes require reheating which could change the properties of the binder. An alternative approach to assessing the long-term performance of WMA pavements is to characterize field cores in the laboratory using performance tests which have been proven to be correlated to long-term field performance (Prowell et al., 2007; Bower et al., 2012). Due to the fact that the WMA projects in U.S. are in the early stages of their design lives and the existing pavement data collection technologies have limitations in data accuracy and data collection speed which poses interruption to traffic flow, the monitoring and evaluating of long-term performance of field WMA mixture is limited thus far. Therefore, a more in-depth understanding of how WMA affects engineering properties of asphalt mixtures and how those properties relate to field performance is needed.

Further, current studies are primarily focusing on quantifying the environmental benefits of WMA. As a matter of fact, the implementation of WMA has implications to environmental, but also economic and engineering benefits. Combined with the long term pavement performance monitoring results, a comprehensive life cycle based assessment of WMA mixtures is currently lacking and should be performed.

The Long Term Pavement Performance (LTPP) Program of Federal Highway Administration (FHWA) recently initiated a new program, Specific Pavement Study 10 (SPS-10), to evaluate the long term performance of WMA mixtures. Under the SPS-10 initiative ("Warm Mix Asphalt Overlay of Asphalt Pavement Study"), the Oklahoma Department of Transportation (ODOT) constructed six LTPP SPS-10 experimental sections on State Highway 66 (SH-66) from 5.95 miles east of United States Route 81 (US-81), extending 4.08 miles to Garth Books Blvd. in Yukon. This new SPS-10 experiment is the testing bed of this study.

1.2 Project Objective

In this project, the state-of-the-art 1mm 3D laser imaging technology named PaveVision3D along with several other instruments and software tools were used to collect pavement surface characteristics data for the ODOT SPS-10 WMA pavement sites on SH-66, and subsequently surface conditions and performance were evaluated. The goal of this study is to evaluate the long term field performance of WMA and to fill the knowledge gap of the long term performance of WMA. Specifically, the objectives of this study are to:

- Perform data collection (including cracking, rutting, roughness, texture, friction) for five years using the OSU 1mm 3D technology and other instruments (a grip tester for friction and a dynamic friction tester (DFT) for friction at highway speed and static setting, and a ultra-high resolution portable LS-40 3D Surface Analyzer and an AMES high-speed profiler for

pavement texture), and evaluate pavement surface characteristics and performance.

- Understand the short-term and long-term performance of the six WMA technologies used in Oklahoma.

1.3 Report Outline

This report documents the LTPP SPS-10 data collection using PaveVision3D and other devices and analysis results of the five years of data collection, aiming to evaluate the surface characteristics of different WMA technologies under traffic. This report consists of five chapters. An overview of each chapter is given below:

- Chapter 1 provides the overall background and objectives of the project.
- Chapter 2 introduces the LTPP SPS-10 in Oklahoma, the testing devices, and ten data collection events (biannually for five years) for this project.
- Chapter 3 presents the measured surface characteristics of the LTPP SPS-10 sites and compares results of different WMA technologies relative to the conventional HMA.
- Chapter 4 proposes several novel macro- and micro-texture indicators for pavement friction evaluation using high-resolution 3D surface texture data.
- Chapter 5 summarizes the conclusions of this study.

CHAPTER 2 LTPP SITE AND DATA COLLECTION DEVICES

To evaluate the long term performance of the LTPP SPS-10 WMA site, 11 data collection efforts had been performed during the past five years, including September 2015 (before the construction), November 2015 (right after the construction), March 2016, May 2016, September 2016, January 2017, July 2017, October 2017, July 2018, March 2019, and June 2019. The PaveVision3D system captured pavement images for cracking and rutting analysis, the AMES Profiler collected pavement roughness and macrotexture data, and the Grip Tester measured pavement friction performance. These three devices are able to perform condition testing at highway speed without interrupting traffic.

2.1 LTPP SPS-10 Site in Oklahoma

The LTPP SPS-10 experiment is designed to evaluate the performance of WMA, both in the short and long term, in relative to the conventional HMA. The experimental matrix should include, at a minimum, one HMA control section and two WMA test sections using foaming process and chemical additive with 10-25% RAP and RAS content. Under the SPS-10 initiative, ODOT constructed six LTPP SPS-10 experimental sections on the westbound of State Highway 66 (SH-66) from 5.95 miles east of US81, extending 4.08 miles to Garth Books Blvd. in Yukon in November 2015. The annual average daily traffic (AADT) on this road is approximately 5,900.

Figure 2.1 ODOT LTPP SPS-10 Site Location

Table 2.1 Experiment Design of ODOT LTPP SPS-10 Site

Section ID	Binder	Comment	Aggregate Combination	AC Content (%)
1	PG 70-28	HMA with RAP + RAS	1	4.9
2	PG 70-28	WMA Foaming with RAP + RAS	1	4.9
3	PG 70-28	WMA Chemical with RAP + RAS	1	5.0
4	PG 64-22	WMA Chemical with RAP + RAS	1	5.0
5	PG 58-28	WMA Chemical with RAP + RAS	1	5.0
6	PG70-28	WMA Stone mix with mineral filler	2	6.6
Mainline	PG70-28	HMA with RAP	3	5.1

Figure 2.1 shows the site location, and Table 2.1 lists the experiment design of the SPS-10 sites, including the binder Performance Grade (PG), aggregate combination for each WMA section and the mainline section (transition between each section), and the asphalt content. As shown in Table 2.1, Sections 1 to 3 are the required SPS-10 experimental designs, while Sections 4 to 6 are the supplemental sections with mixes chosen by the ODOT Division Office. Sections 1 to 3 were constructed with the same aggregate combination, but for the conventional HMA control section, WMA using Astec double barrel green (foaming process) and Evotherm M1A (chemical additive). Sections 4 and 5 were constructed with the same aggregate combination using Evotherm M1A but different binder grades.

Section 6 was constructed with stone matrix asphalt (SMA) but without fibers (typically used to combat drain down issues).

The gradation curves of the aggregate combinations are shown in Figure 2.2. Aggregate Combination 1 contains 38% 5/8 Chips + 35% Stone Sand + 12% Sand + 12% RAP + 3% RAS; Aggregate Combination 2 contains 90% 5/8 Chips + 10 Mineral Filler; and Aggregate Combination 3 contains 34% 5/8 Chips + 13% Scrns. + 30% Stone Sand + 13% Sand + 10% RAP. The gradation of aggregate combination 1 and 3 is close to each other, whereas the aggregate combination 2 for the WMA SMA site is distinctively different. All the gradations of the mixes meet the corresponding specification requirements at ODOT.

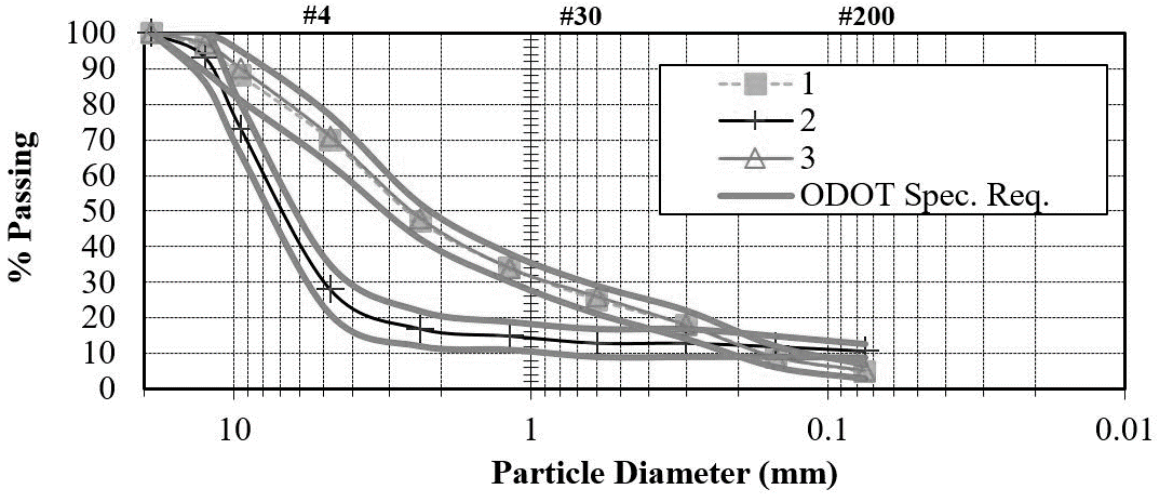

Figure 2.2 Gradation Curves for Aggregate Combinations

2.2 Testing Devices

Three high speed devices (PaveVision3D, AMES Profiler, and Grip Tester) were used for the data collection in this research. By October 2019, ten data collection events were conducted on the six LTPP SPS-10 experimental sections after the construction. Pavement cracking, rutting, roughness, macrotexture and friction data were obtained at highway speed without interrupting the traffic.

2.2.1 PaveVision3D Ultra System

The PaveVision3D laser imaging system has evolved into a sophisticated system to conduct full lane data collection on roadways at highway speeds up to 60mph (96.5 km/h) at 1mm resolution (Wang et al., 2015). Figure 2.3 demonstrates the Digital Highway Data Vehicle (DHDV) equipped with PaveVision3D system. The system is able to acquire both 3D laser imaging intensity and range data from pavement surfaces through two separate sets of sensors. Two 3D high resolution digital accelerometers have been integrated in the system, capable of reporting compensated pavement surface profiles and generating roughness indices. The collected data are saved as image frames with the dimension of 2,048 mm in length and 4,096 mm in width. In summary, the 1mm 3D pavement surface data can be used for:

- Comprehensive evaluation of surface distresses: automatic and interactive cracking detection and classification based on various cracking protocols;
- Profiling: transverse for rutting and longitudinal for roughness (Boeing Bump Index and International Roughness Index);

- Safety analysis: including macrotexture in term of mean profile depth (MPD) and mean texture depth (MTD), hydroplaning prediction, and grooving identification and evaluation;
- Roadway geometry: horizontal curve, longitudinal grade, cross slope.

Figure 2.3 DHDV with PaveVision3D System

2.2.2 AMES 8300 Survey Pro High Speed Profiler

The Model 8300 Survey Pro High Speed Profiler (Figure 2.4) is designed to collect macro surface texture data along with standard profile data at highway speeds. The International Roughness Index (IRI) is calculated from the pavement profile data. Multiple texture indices such as Mean Profile Depth (MPD) can be calculated from the testing data. This High Speed Profiler meets or exceeds the following requirements: ASTM E950 Class 1 profiler specifications, AASHTO PP 51-02 and Texas test method TEX 1001-S. The texture specifications of the Profiler include:

- Capable of collecting measurements at speeds between 25 and 65 mph;

- Laser height sensor with a range of 180 mm and a resolution of 0.045 mm;
- Horizontal distance measured with an optical encoder that has a resolution of 1.2 mm;
- Pavement elevation sampling rate 62,500 samples per second;
- Profile wavelength down to 0.5 mm.

Figure 2.4 AMES 8300 Survey Pro Profiler

2.2.3 Grip Tester (ASTM E274)

Grip Tester (Figure 2.5), which follows the ASTM E274 - 11 "Standard Test Method for Skid Resistance of Paved Surfaces Using a Full-Scale Tire", has been used in recent years by FHWA on many demonstration projects in U.S. It is designed to continuously measure the longitudinal friction along the wheel path operating around the critical slip of an anti-braking system (ABS) across the entire stretch of a road with much lower water consumption. Grip Tester is able to provide greater details about spatial variability of friction data and is an ideal option for

project and network level friction management. The device has the capability to test at highway speeds (60 mph / 100 km/h) as well as low speeds (20 mph / 32 km/h) using a constant water film thickness. The collected data are recorded in 3-ft (0.9 m) intervals by default and can be adjusted by the user.

Figure 2.5 Grip Tester

CHAPTER 3 PERFORMANCE EVALUATION

Data sets collected before the SPS-10 site construction and the subsequently ten collection events during the past five years are analyzed and the pavement surface characteristics of WMA and HMA sections are compared in this chapter to evaluate their long term field performance. The following performance results are summarized:

- Pavement cracking and rutting data (collected by the PaveVision3D System);
- Pavement macrotexture and roughness (IRI) data (collected by the AMES® Profiler);
- Pavement friction data (collected by the Grip Tester).

3.1 Pavement Cracking

The images obtained by the PaveVision3D system from the LTPP SPS-10 site were analyzed to detect pavement cracking. On each section, cracking information was summarized for each data collection and the time series data were compared to evaluate the development of cracking over time. The 3D Automated Distress Analyzer (ADA3D) is an automatic analyzing tool to report pavement condition data from the PaveVision3D collected images. By implanting the sophisticated algorithms, the ADA3D (Figure 3.1) is capable of conducting automated cracking, rutting, roughness, and texture analyses at 1 mm resolution.

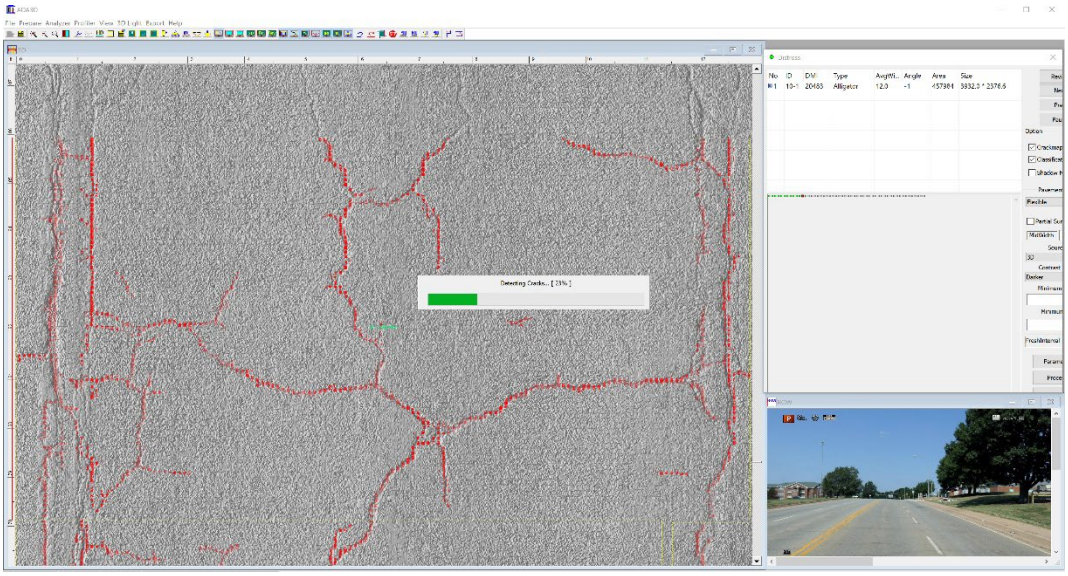

Figure 3.1 Interface of ADA3D

To obtain cracking data for each WMA or HMA section within the LTPP SPS-10 site, the research team made several changes in the ADA3D software as follows:

- Automatic lane marking detection. The ADA3D software can automatically identify lane for each image frame, so that only the cracks within each lane are detected for consistent comparisons among the various data collection.
- Deep Learning (DL) based cracking detection. The DL algorithm is able to automatically detect cracking from pavement images with minimum human interaction.
- Reporting of Cracking Percent. The customized ADA is able to generate wheel path and grids to compute Cracking Percent, a measure representing the cracking extent and severity of a pavement section.

3.1.1 Automatic Lane Marking Detection

Pavement longitudinal lane markings define traffic lanes moving in the same or opposite directions. To be consistent, it is desired to report cracks within a lane, and thus the identification of lane markings is important.

A match filter based method is implemented in the ADA3D software to automatically detect lane markings based on the collected 2D pavement images from the PaveVision3D system (Zhang et al., 2018). To evaluate the efficiency of the proposed algorithms, various pavement testing sections with a total length roughly 38,000 feet were surveyed and selected for algorithm validation. It was demonstrated that the ADA3D software could achieve the F-measures of 96%, 94.2%, and 82% when the pavement lane markings were in excellent, fair, and poor conditions. Figure 3.2 shows typical performances of the lane marking detector. Image area within the lane markings is used for the following cracking analysis.

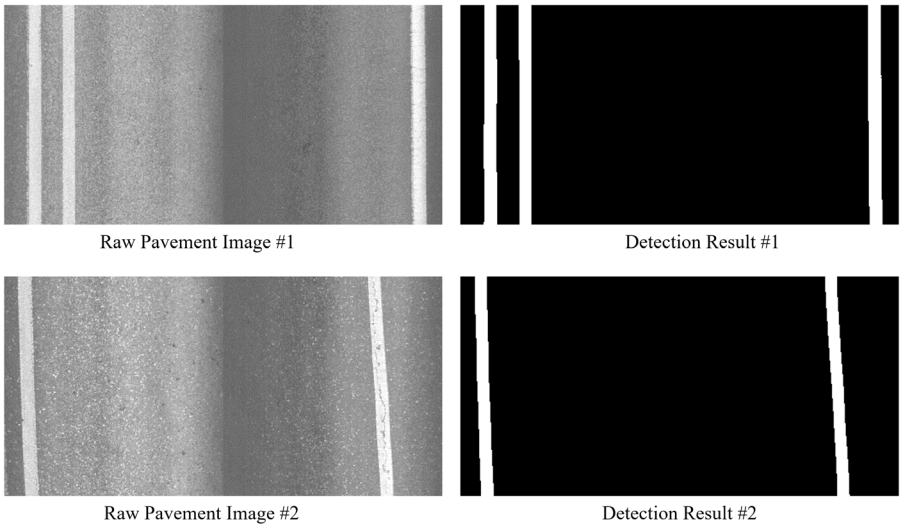

Figure 3.2 Illustration of Lane Marking Detection (Zhang et al., 2018)

3.1.2 Deep Learning based Cracking Detection

Once lane markings are detected, the ADA3D software will analyze the image areas for cracking detection. Specifically, Deep Learning (DL) based cracking detection algorithm, *CrackNet*, has been implemented in ADA3D to automatically detect cracks and acquire the corresponding cracking data with minimum human interaction (Zhang et al, 2017). The reason to switch to the innovative DL approach is that traditional computer based imaging techniques are not able to provide needed and consistent precision and bias levels for automated cracking survey.

Training of a DL-based network is extremely tedious and slow and requires substantial manpower. The training samples include approximately 3,000 high-resolution 3D pavement surfaces being manually marked for cracking, and an elaborate manual QA process is applied to ensure the data quality of the training samples. Training samples were acquired not only in Oklahoma but also form a dozen other states. The cracking detection results from the DL initiative are leaps-and-bounds better than past efforts using traditional algorithms.

The architecture of *CrackNet*, as illustrated in Figure 3.3, is constituted of five layers of neuron networks: two fully-connected layers, one convolution layer, one 1 by 1 convolution layer and one output layer. The input of *CrackNet* are 360 feature maps generated by the feature extractor. Each feature map has the same size with the input image. The fully-connected layers I and II provide full connections to previous layers following a pixel-independent manner. More than a million parameters were finally obtained after the training of *CrackNet*. Using this DL

architecture, the precision and recall of automated cracking detection can consistently achieve 90% in validation tests.

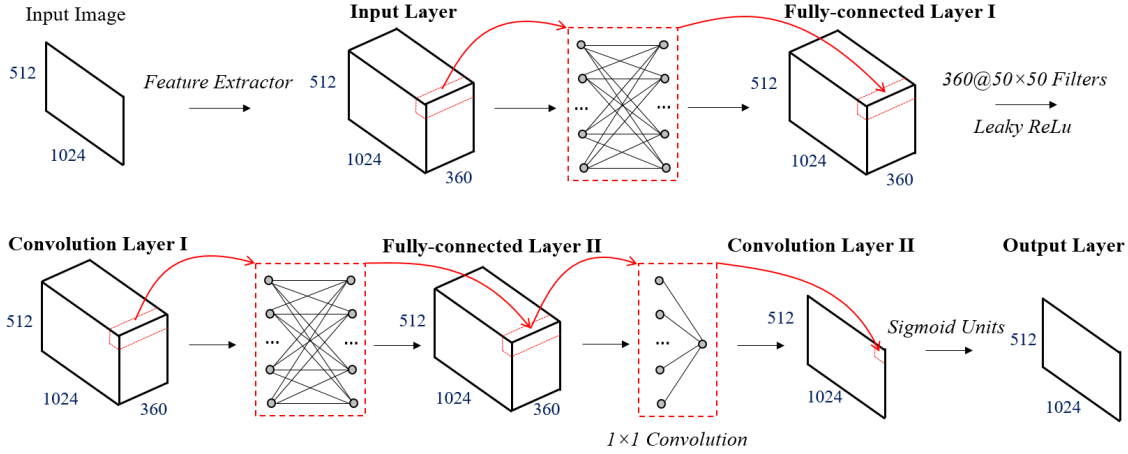

Figure 3.3 DL Architecture of CrackNet (Zhang et al. 2017)

3.1.3 Reporting of Cracking Percent

Cracking Percent computes the percent of cracking within the lane markings of a pavement section. This definition defines the overall cracking extent of a pavement and is used to compute percent of WMA or HMA section which has been affected by cracking. The roadway surface is divided into 10 in. by 10 in. (250 mm by 250 mm) grid squares (as shown in Figure 3.4), and the Cracking Percent is calculated as below:

$$CrackingPercent = \frac{n_c}{N} \times 100\% \tag{3.1}$$

Where n_c is the number of 10 in. by 10 in. (250 mm by 250 mm) grids containing cracks, while N is the total number of 10 in. by 10 in. (250 mm by 250 mm) grids for a WMA or HMA pavement section.

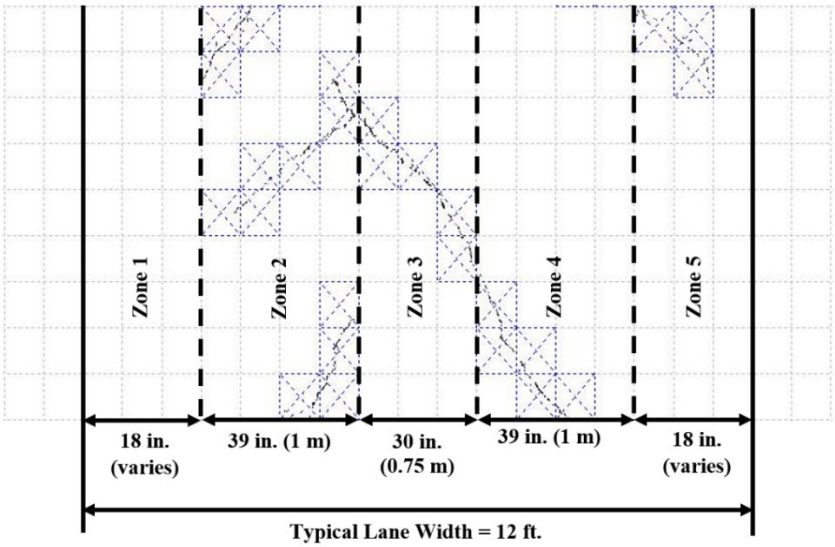

Figure 3.4 Wheel Path definitions and 10 in. by 10 in. (250 mm by 250 mm) Grids

In addition, the average crack width in each grid are used as the severity measurement. The most common two severity thresholds are: 0.25 in. (6 mm) and 0.50 in. (12 mm, which defines the three cracking severities: low (L), medium (M), and high (H). For each grid with the size of 10 in. by 10 in. (250 mm by 250 mm), the average width of cracking is computed as a single value. The percentage of grids within each of the three severities for each section of the LTPP SPS-10 site is summarized.

Therefore, a total of four statistics are generated to represent pavement cracking condition: Cracking Percent and three values representing the percentages of cracked grids for the three severity levels. For instance, for the data collection in June 2019 on Section 4, the Cracking Percent is 12.63%, while 11.40% is low severity, 1.23% is medium severity, and 0.00% is high severity.

Once the lane markings are determined, the ADA3D software will generate two wheel-paths and 10 ft. by 10 feet grids on each image frame and summarize the cracking information for each pavement section (as shown in Figure 3.4). Wheel paths are defined as a longitudinal pavement strip with 39 in. (1 m) in width. The two wheel paths are separated by a 30 in. (0.75 m) median zone. It is proposed to have 10 in. by 10 in. (250 mm by 250 mm) square grids for Cracking Percent computation so that the layout for wheel paths and the median would not have partial grids. The grid layout for areas outside of both wheel paths starts from the edges of the wheel paths. Lane markings themselves are not included in any of the five zones.

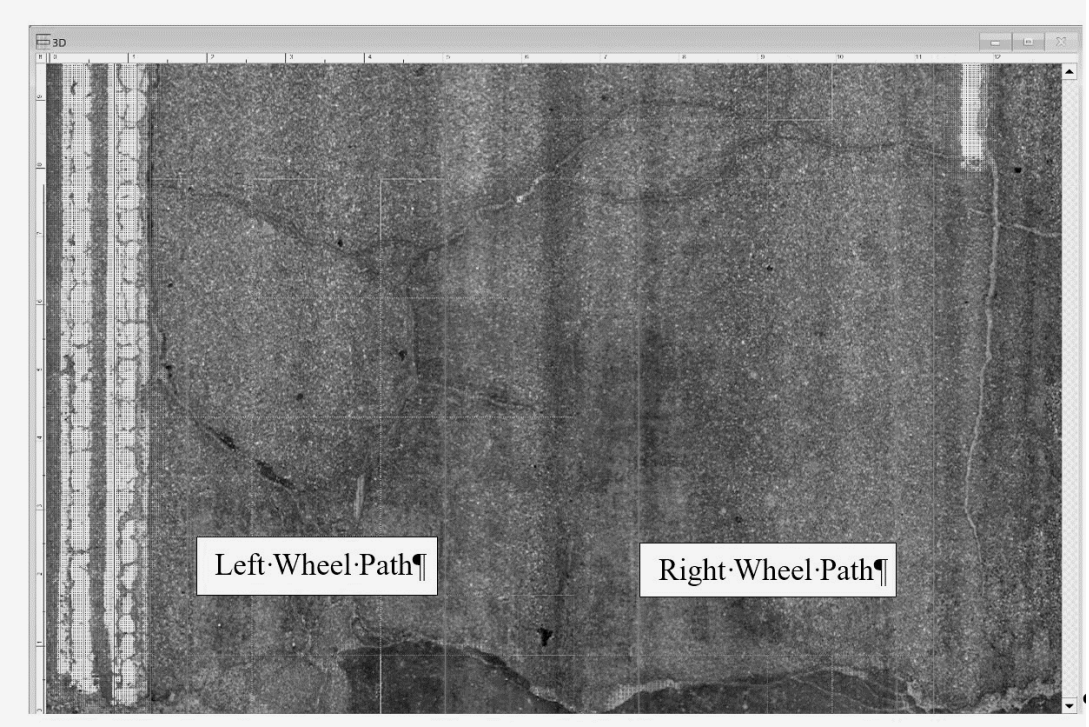

Figure 3.5 Example Image Frames with Wheel Paths and Grids

Figure 3.5 illustrates an example pavement images with wheel paths and grids. The lane markings are automatically determined by the software and

highlighted in blue color. The left and right wheel paths are defined with two blue lines. The 10 in. by 10 in. (250 mm by 250 mm) grids with cracking are displayed herein: a grid with a “red dot” indicates it has high severity cracking and the average crack width is larger than 0.50 in. (12 mm); a grid with a “yellow dot” means it has a medium severity cracking and the average crack width lies between 0.25 in. (6 mm) and 0.50 in. (12 mm); and a grid with a “blue dot” means it has a low severity cracking and the average crack width is less than 0.25 in. (6 mm). Finally, if no lane markings appear on some pavement images, the software applies “default lane width” to define the image area for cracking detection. The area between the two blue lines in Figure 3.5 will represent the “default lane width” for images without lane markings.

3.1.4 Cracking Results

3.1.4.1 Before Construction

Right before the construction, large amount of sealed cracking were observed on the testing site on SH-66 (as shown in Figure 3.6.a). The ADA3D software is able to detect those cracking that are not covered by sealants (as shown in Figures 3.6.b and 3.6.c).

The Cracking Percent on each section before construction (September 2015) are summarized in Figure 3.7 and Table 3.1. Before construction, the Cracking Percent were 11.89%, 16.13%, 11.48%, 11.62%, 35.65%, and 20.02% for Sections 1 to 6. In addition, the Cracking Percent at different severity levels on each section is displayed in Figure 3.7.b. Most of the cracking on these sections had an average crack width larger than 0.5 in. (12 mm) which belong to the high severity level. The

Low Severity Cracking Percent were 1.01%, 1.32%, 1.12%, 0.99%, 2.44%, and 1.60% for Sections 1 to 6; while the High Severity Cracking Percent for those sections were 8.66%, 12.62%, 7.97%, 8.68%, 28.33%, and 15.29%.

Therefore, before construction, Section 5 of the existing pavement had the highest Cracking Percent, followed by Section 6 and Section 2. Sections 1, 3 and 4 had comparable Cracking Percent values.

Table 3.1 Cracking Percent Before Construction (%)

Severity Levels	Section 1	Section 2	Section 3	Section 4	Section 5	Section 6
Total	11.89	16.13	11.48	11.62	35.65	20.02
Low	1.01	1.32	1.12	0.99	2.44	1.60
Medium	2.22	2.19	2.39	1.96	4.88	3.12
High	8.66	12.62	7.97	8.68	28.33	15.29

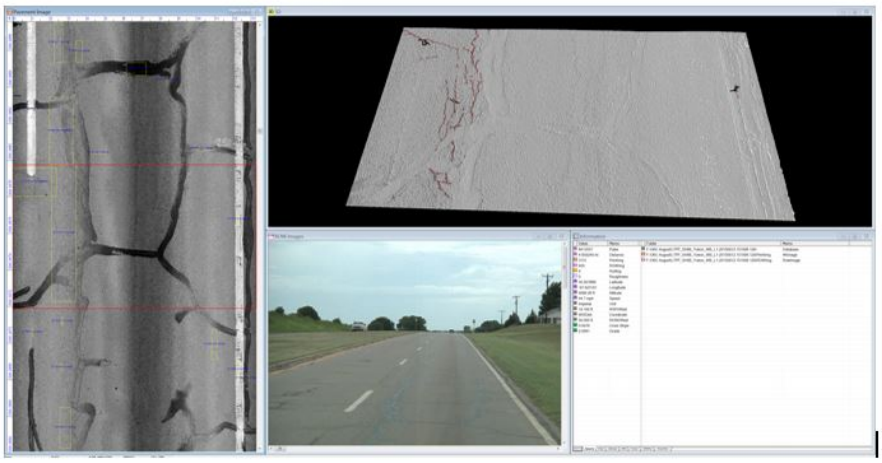

(a) Right-of-Way (ROW) Image

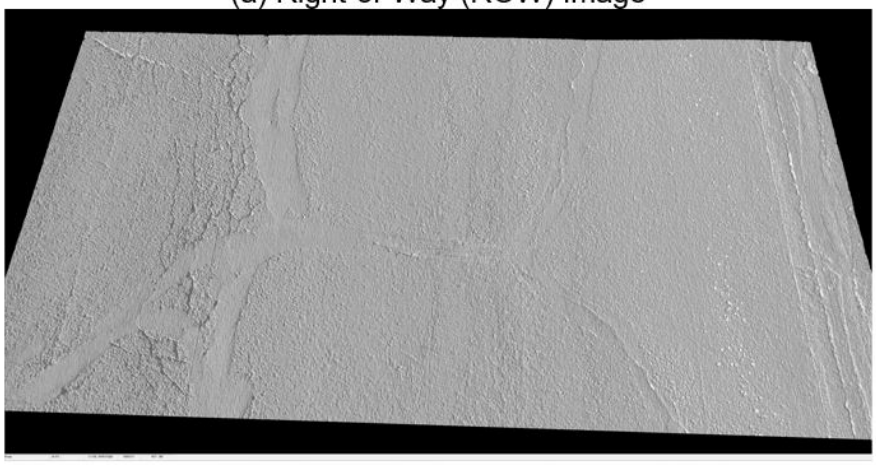

(b) 3D Raw Data

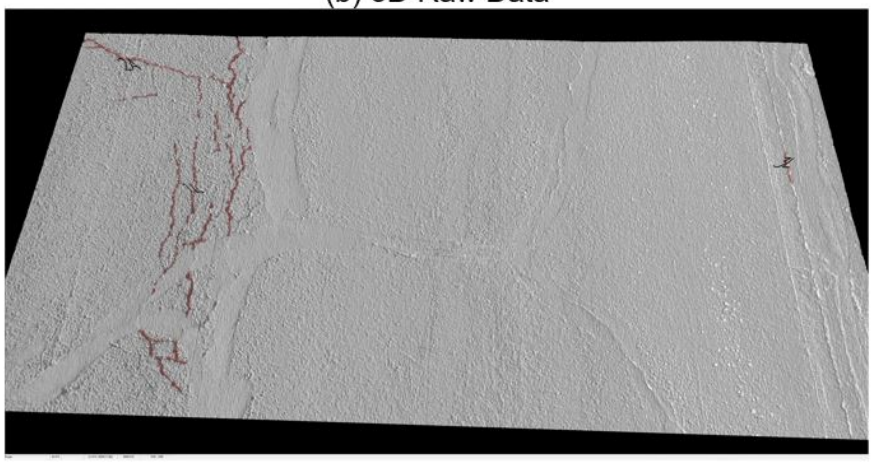

(c) Crack Detection Result

Figure 3.6 Example Images before Construction

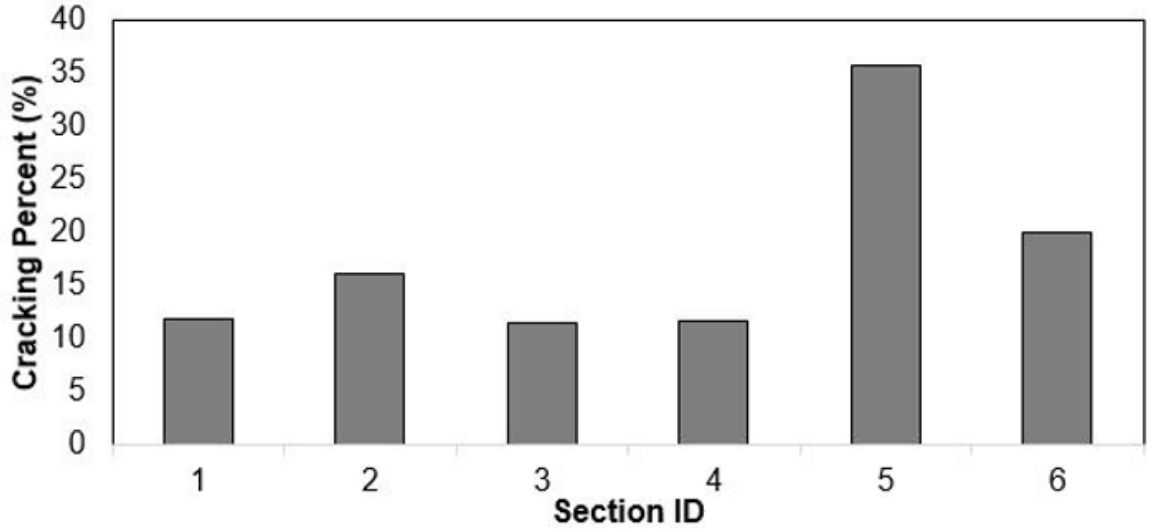

(a) Cracking Percent

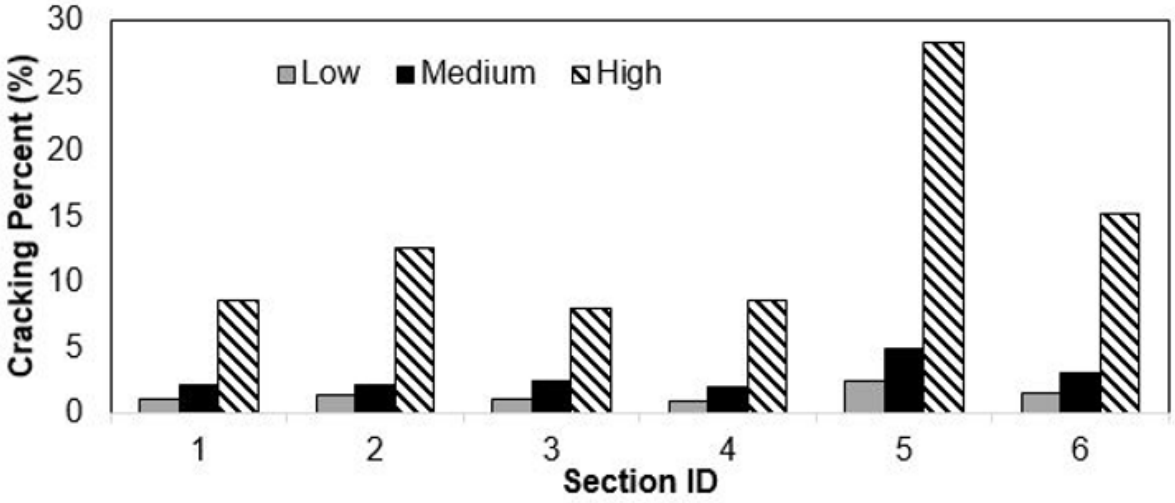

(b) Different Severity Levels

Figure 3.7 Cracking Percent before Construction

3.1.4.2 After Construction

After the LTPP SPS-10 was constructed, no cracking was detected on all the six sections during the first five data collections (from November 2015 to January

2017). In other words, the WMA and HMA pavements were free of cracking distress in the first two years of service.

Starting from July 2017, cracking appeared on the pavement surfaces, especially on Section 4. However, these sections exhibit different trend in terms of cracking development. Figures 3.8 to 3.12 provides example pavement images with cracking developed over time on Sections 1 to 4 at the same locations. For Sections 1, 2, and 3, the cracking was not showing until October 2017 (Figures 3.8, 3.9, and 3.10), while Section 4 started showing minor cracks during data collection in July 2017 (Figures 3.11 and 3.12). For Sections 5 and 6, no cracking was found up to June 2019, the last data collection event for this project.

In addition, it is worth mentioning that most of the cracking observed on the sections up to June 2019 are transverse tracking. Since the climate and traffic load conditions are identical for these six sections, the difference in cracking performance should be due to the various mixture design, as introduced in Table 2.1.

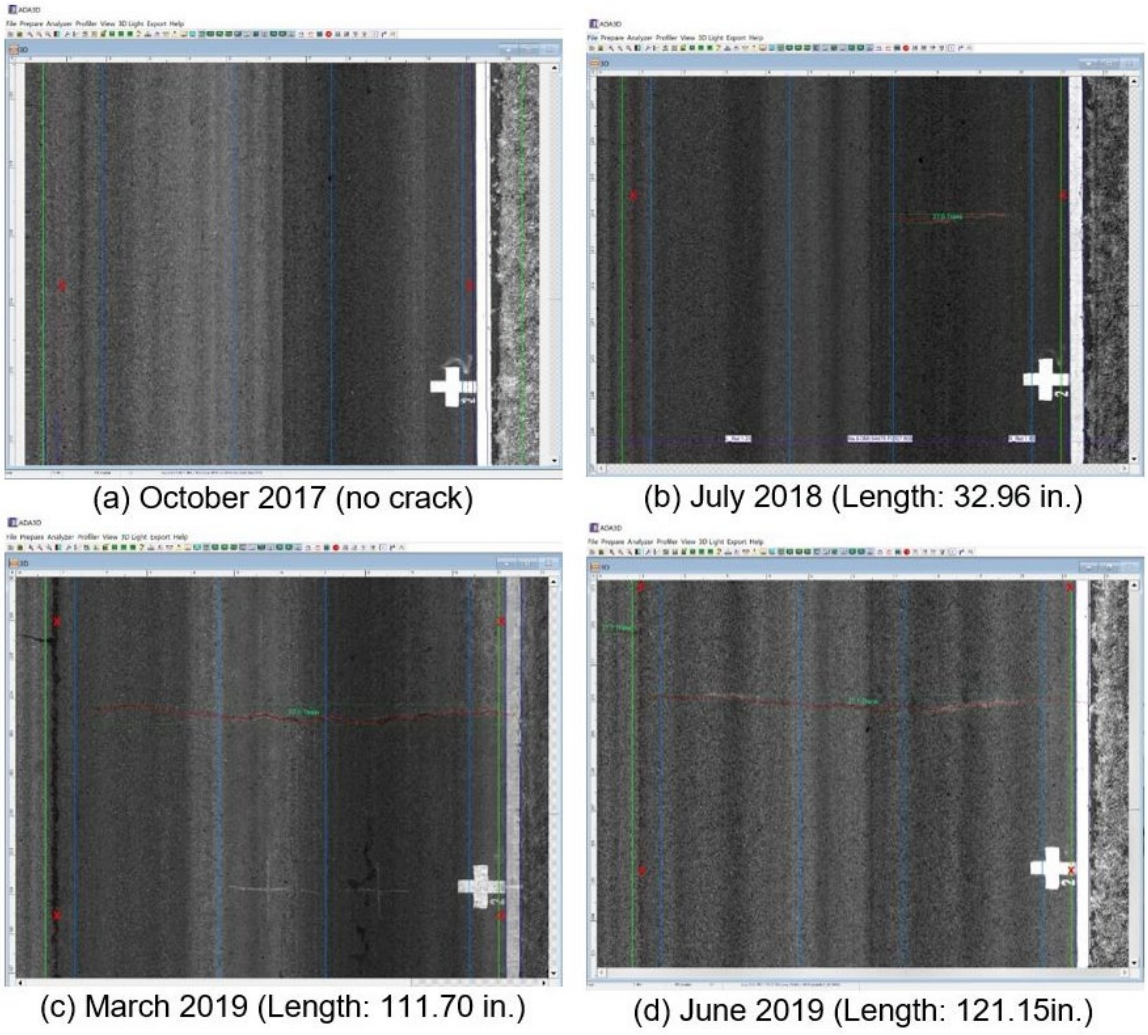

Figure 3.8 Crack Development on Section 1 (around +200 ft.)

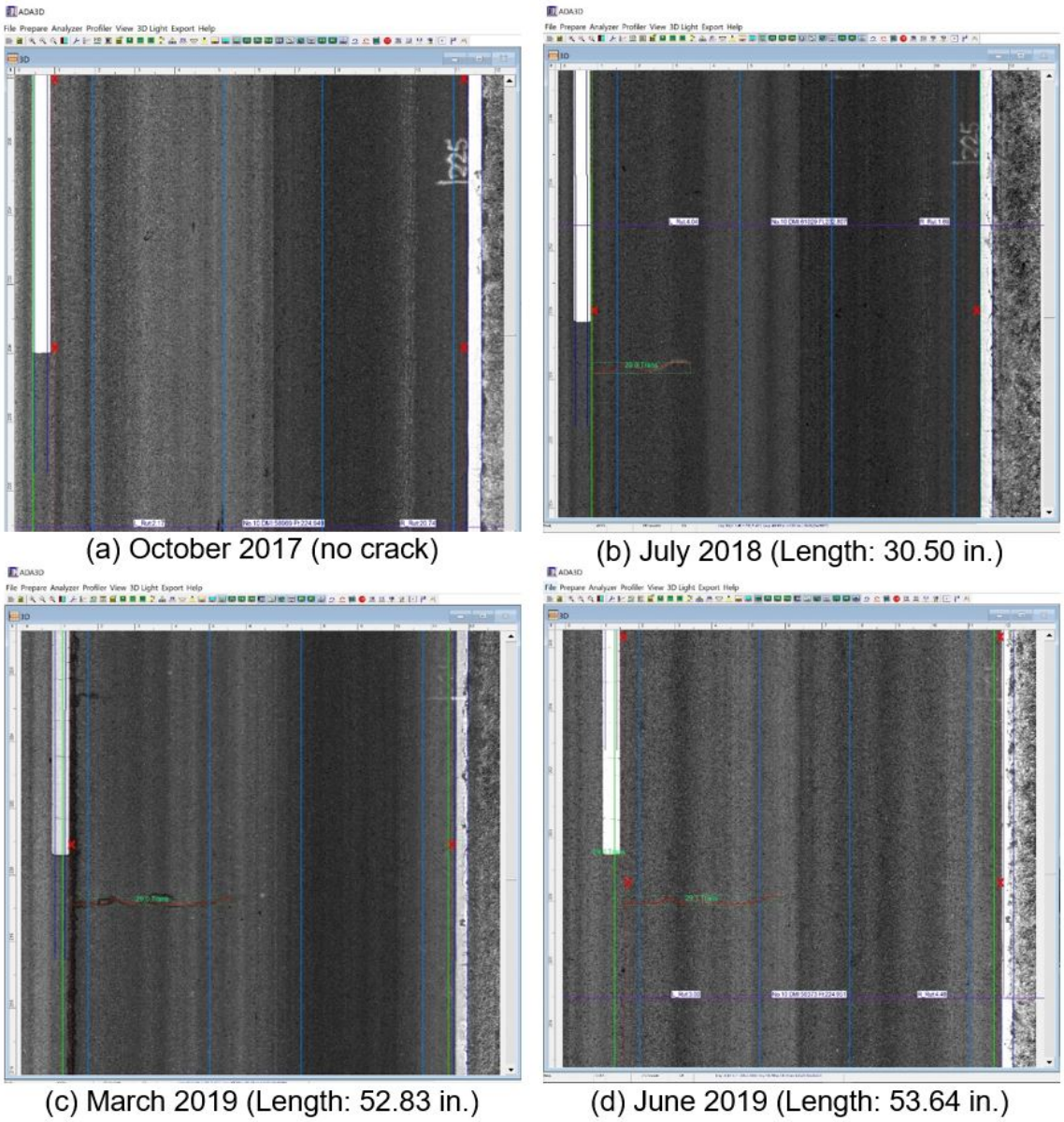

(a) October 2017 (no crack)

(b) July 2018 (Length: 30.50 in.)

(c) March 2019 (Length: 52.83 in.)

(d) June 2019 (Length: 53.64 in.)

Figure 3.9 Crack Development on Section 2 (around +225 ft.)

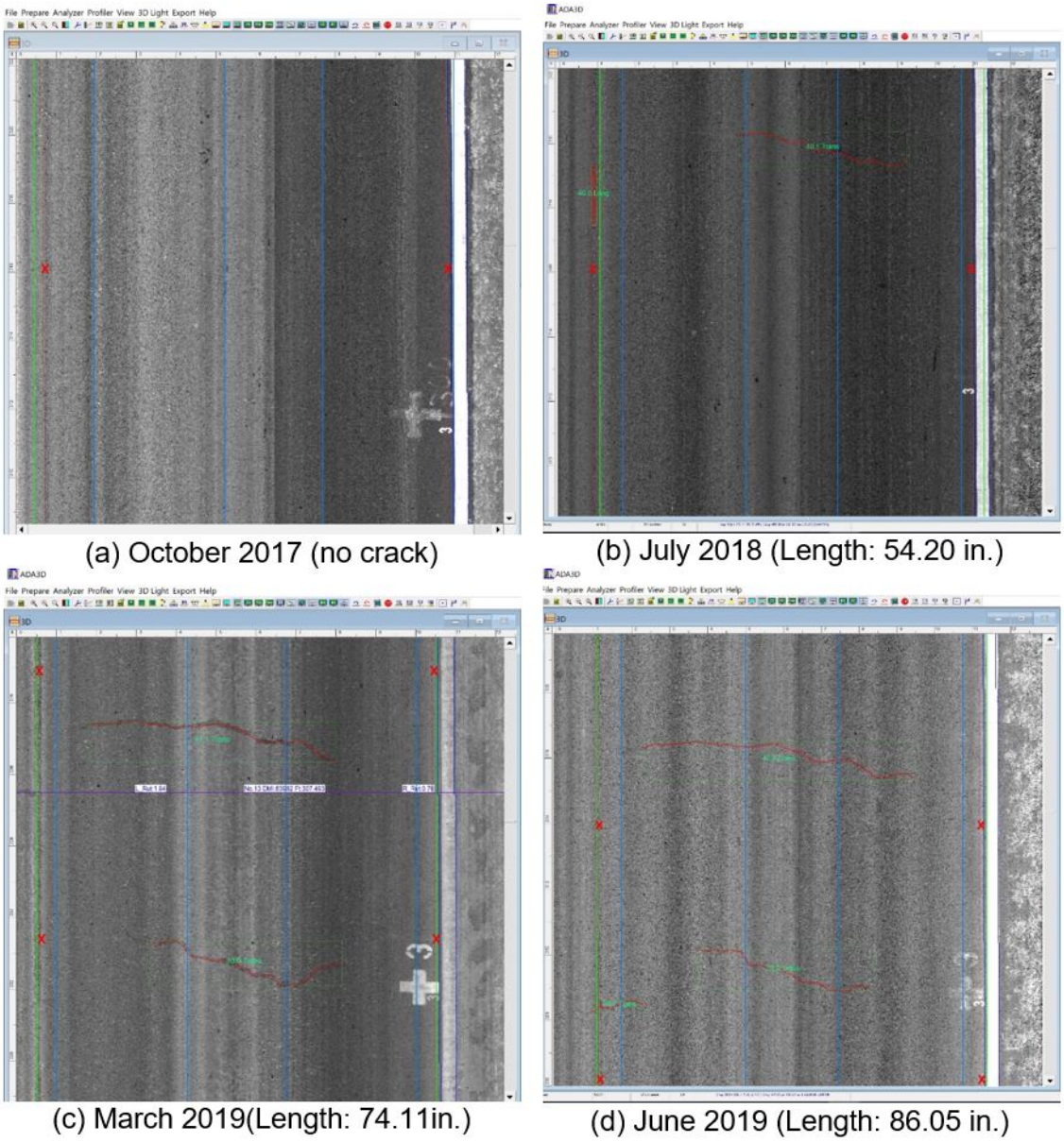

Figure 3.10 Crack Development on Section 3 (around +300 ft.)

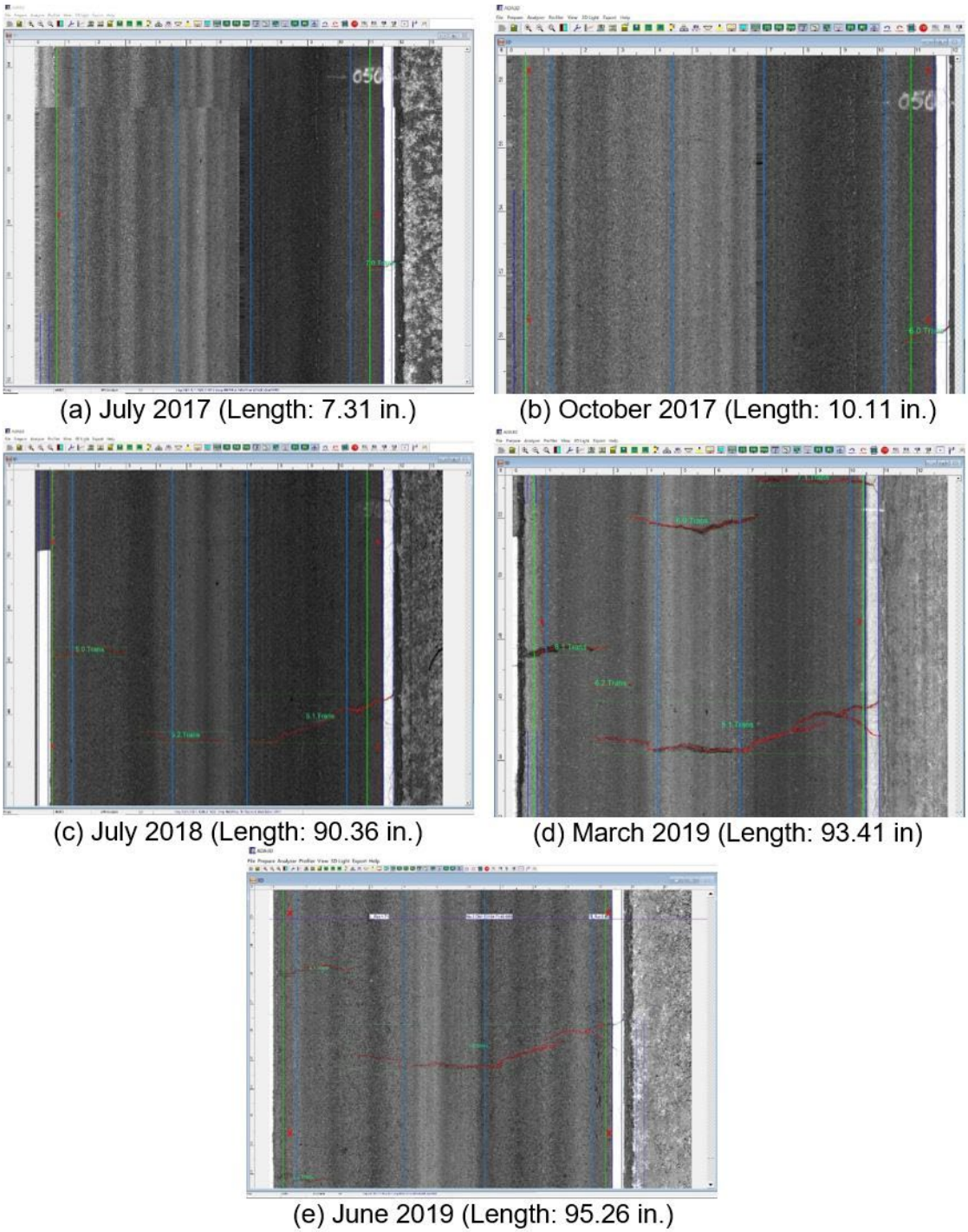

(a) July 2017 (Length: 7.31 in.)

(b) October 2017 (Length: 10.11 in.)

(c) July 2018 (Length: 90.36 in.)

(d) March 2019 (Length: 93.41 in)

(e) June 2019 (Length: 95.26 in.)

Figure 3.11 Crack Development on Section 4 (around +50 ft.)

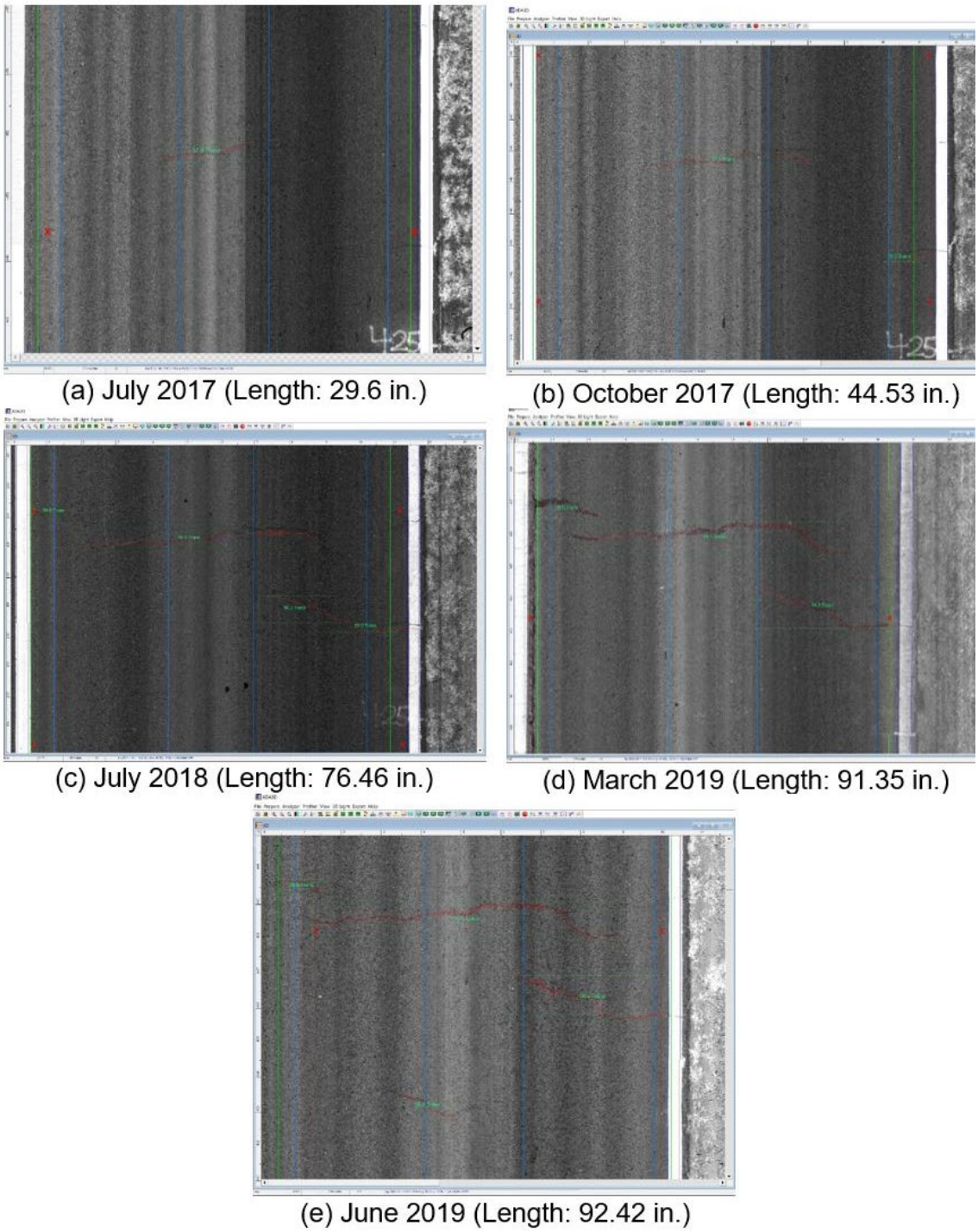

Figure 3.12 Crack Development on Section 4 (around +425 ft.)

The Cracking Percent for each section during the project period since July 2017 are summarized in Figure 3.13 and Table 3.2. By the end of the fifth year (from data collection in June 2019), the Cracking Percent were 5.39%, 5.23%, 5.53%, 12.63%, 0%, and 0% for Sections 1 to 6. Therefore, Sections 2 and 3 (WMA) showed comparable cracking performance as Section 1 (HMA control), Section 4 (WMA) demonstrated significant amount of cracking performance as compared to the control HMA section (Section 1), while Sections 5 and 6 (WMA) have not showed any cracking on the surface.

Table 3.2 Cracking Percent over Time

Testing Time	Section 1	Section 2	Section 3	Section 4	Section 5	Section 6
Jul-17	0.00	0.00	0.00	0.71	0.00	0.00
Oct-17	0.00	0.00	0.00	1.63	0.00	0.00
Jul-18	1.30	0.97	0.60	7.29	0.00	0.00
Mar-19	5.02	5.64	5.34	11.19	0.00	0.00
Jun-19	5.39	5.23	5.53	12.63	0.00	0.00

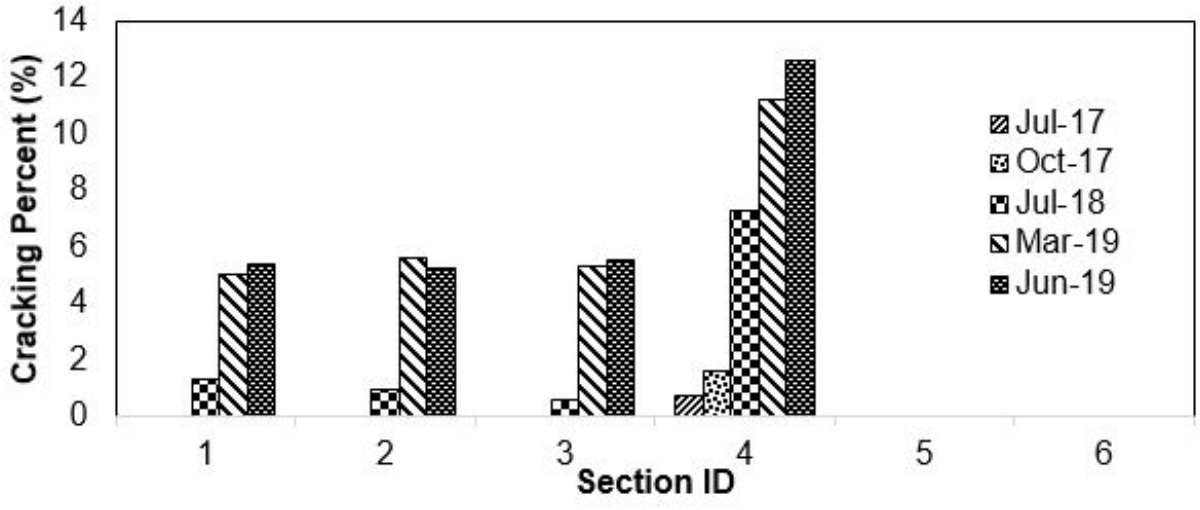

Figure 3.13 Cracking Percent over Time

In addition, the Cracking Percent at different severity levels on each section for all data collection events since July 2017 are summarized in Figure 3.14 and Table 3.3. Most of the cracking developed on Sections 1 to 4 had an average crack width less than 0.25 in. (6 mm) which lie in the low severity level. For the data collection in June 2019, the Low Severity Cracking Percent were 5.39%, 5.18%, 5.52%, 11.40%, 0%, and 0% for Sections 1 to 6. As shown in Figure 3.14.b, Section 4 had showed medium severity cracking while other sections have not. No cracking with high severity levels are observed thus far, and therefore the data results are omitted. Again, in terms of Cracking Percent at different severity levels, comparing to the conventional HMA (Section 1), Sections 2 and 3 (WMA) showed comparable performance, Section 4 (WMA) was the worst performer, and Sections 5 and 6 (WMA) exhibited the best performance without any cracks observed.

Table 3.3 Cracking Percent at Different Severity Levels over Time

Severity Level	Testing Time	Section 1	Section 2	Section 3	Section 4	Section 5	Section 6
Low	Jul-17	0.00	0.00	0.00	0.71	0.00	0.00
Low	Oct-17	0.00	0.00	0.00	1.63	0.00	0.00
Low	Jul-18	1.29	0.97	0.60	7.20	0.00	0.00
Low	Mar-19	5.01	5.64	5.34	11.12	0.00	0.00
Low	Jun-19	5.39	5.18	5.52	11.40	0.00	0.00
Medium	Jul-17	0.00	0.00	0.00	0.00	0.00	0.00
Medium	Oct-17	0.00	0.00	0.00	0.00	0.00	0.00
Medium	Jul-18	0.00	0.00	0.00	0.09	0.00	0.00
Medium	Mar-19	0.01	0.00	0.00	0.08	0.00	0.00
Medium	Jun-19	0.00	0.05	0.00	1.23	0.00	0.00

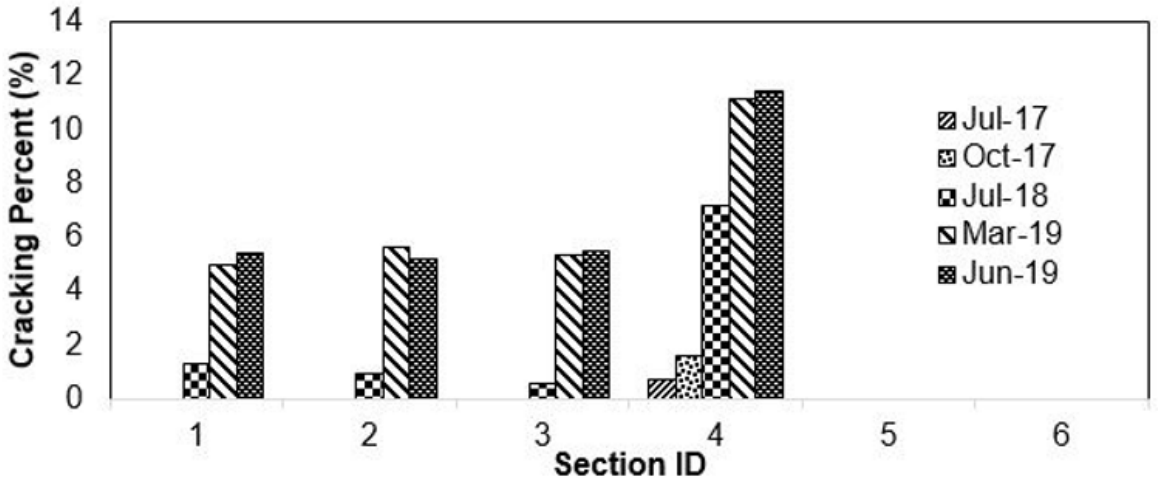

(a) Low Severity Cracking Percent

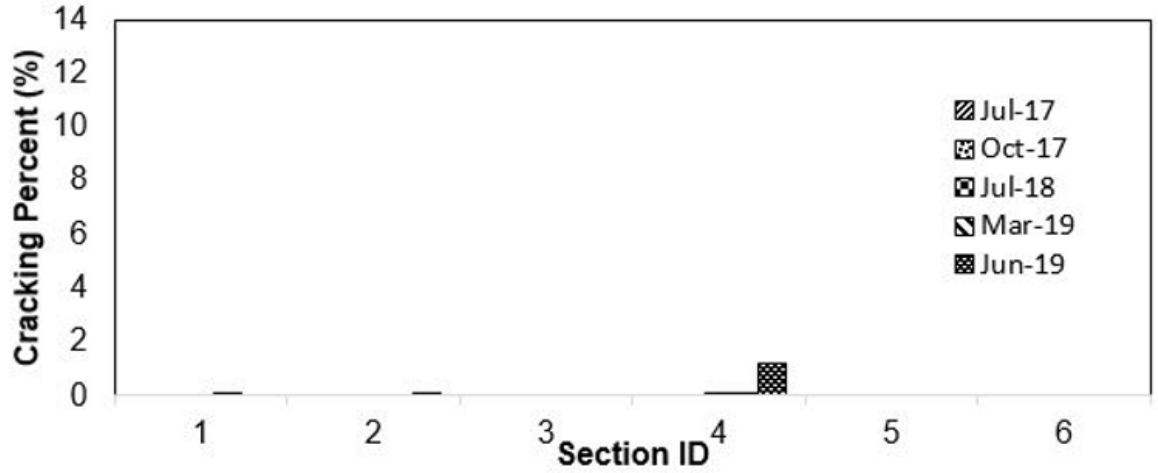

(b) Medium Severity Cracking Percent

Figure 3.14 Cracking Percent at Different Severity Levels over Time

Subsequently, comparisons of these sections were performed before and after the SPS-10 construction. It seems that the pavement condition before construction did not affect the development of pavement cracking of the WMA sections. Combined with the mixture design information in Table 2.1, the cracking performance of each WMA section is detailed below:

- Sections 2 (WMA Foaming with RAP + RAS) and 3 (WMA Chemical with RAP + RAS) achieve comparable cracking performance as Section 1

(control HMA mix with RAP + RAS), as they have the same binder grade (PG 70-28), aggregate gradation (Combination 1), and AC content (4.9% to 5.0%). It indicates WMA could perform like the traditional HMA mixes in terms of cracking performance if constructing with the same mixture design;

- Section 4 (WMA Chemical with RAP + RAS) and Section 1 (HMA with RAP + RAS) have the same aggregate gradation (Combination 1) and AC content (5.0%), but different binder types (PG 64-22 vs. PG 70-28). The low temperature of binder PG 64-22 of Section 4 is 6°C higher than PG 70-28 used in Section 1. Among the six section, Session 4 is the only session using -22°C (low temperature) binder, while all the others use -22°C. Therefore, Section 4 is less resistance to thermal cracking as compared with Section 1 and displays the worse cracking performance. It agrees with previous findings that “fewer percent of pavements with significant amounts of transverse cracking are represented by mixes with -34 binder grades as compared to those with -28 binder grades” (Dave et al., 2015);
- Section 5 (WMA Chemical with RAP + RAS) and Section 1 (HMA with RAP + RAS) have the same aggregate gradation (Combination 1) and AC content (5.0%), but different binder (PG 58-28 vs. PG 70-28). The high temperature of binder PG 58-28 of Section 5 is 12 °C lower than PG 70-28 used in Section 1, which should impacts its high temperature related

performance such as rutting. Additional work is needed to justify why Section 5 demonstrated better cracking performance than Section 1;

- Different from Section 1 (HMA with RAP + RAS) with traditional mix design, Section 6 (WMA Stone mix with mineral filler) was designed with the ODOT SMA specification containing very different gradation and AC content (6.6% vs. 4.9%). It is therefore desired to have better cracking performance on section 6 than that on Section 1, which is in accordance with the findings in previous research (Dave et al., 2015).

3.2 Pavement Rutting

Rutting is defined as the permanent traffic-associated deformation within asphalt pavement layers. The recent provisionally-approved AASHTO Designation PP69-10 (AASHTO, 2013b), “Standard Practice for Determining Pavement Deformation Parameters and Cross Slope from Collected Transverse Profiles”, has been implemented into the PaveVision3D system for rutting characterization. For the 11 data collections before and after the SPS-10 construction, rutting in the left and right wheel-paths are calculated in ADA3D and averaged on each section, as shown in Figure 3.15 and Table 3.4.

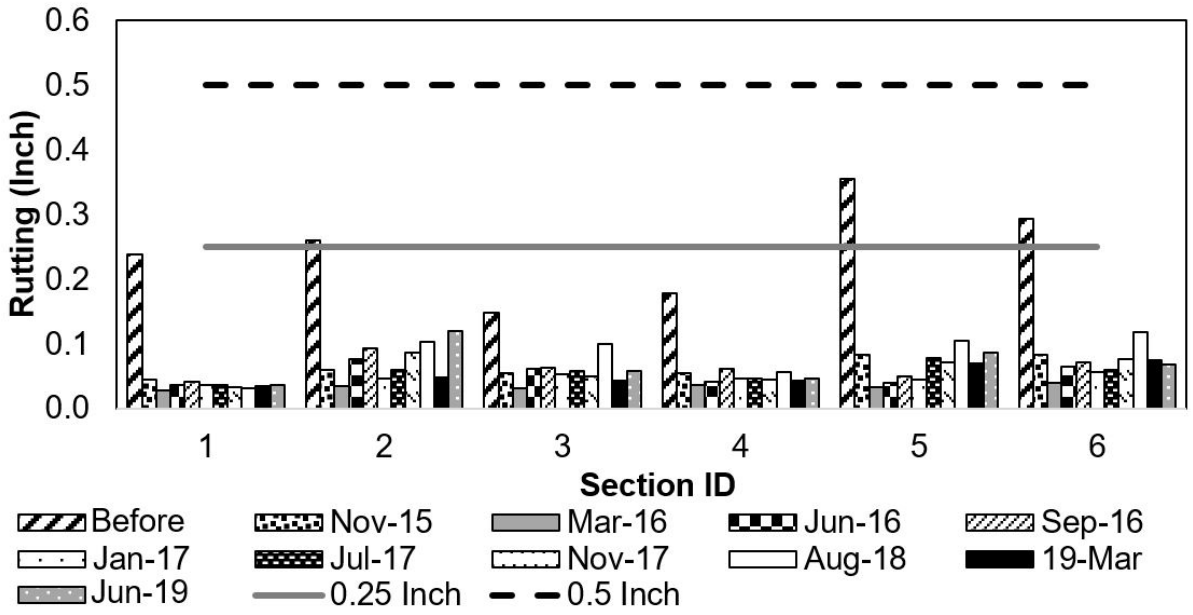

Figure 3.15 Rutting Values over Time

Table 3.4 Rutting Values of Each Section (inch) over Time

Testing Time	Section 1	Section 2	Section 3	Section 4	Section 5	Section 6
Before	0.24	0.26	0.15	0.18	0.35	0.29
Nov-15	0.05	0.06	0.05	0.05	0.08	0.08
Mar-16	0.03	0.03	0.03	0.04	0.03	0.04
Jun-16	0.04	0.08	0.06	0.04	0.04	0.07
Sep-16	0.04	0.09	0.06	0.06	0.05	0.07
Jan-17	0.04	0.05	0.05	0.05	0.04	0.06
Jul-17	0.04	0.06	0.06	0.05	0.08	0.06
Oct-17	0.03	0.09	0.05	0.05	0.07	0.08
Jul-18	0.03	0.10	0.10	0.06	0.11	0.15
Mar-19	0.03	0.05	0.04	0.04	0.07	0.07
Jun-19	0.04	0.12	0.06	0.05	0.09	0.07

According to the ASTM D6433 (2018), “Standard Practice for Roads and Parking Lots Pavement Condition Index Surveys”, average rutting values of 0.25 inches and 0.5 inches could be classified as low and high severity levels. On these

sections, the average rutting values before construction were 0.24, 0.26, 0.15, 0.18, 0.35 and 0.29 inches respectively. In other words, before the construction, Section 5 of the existing pavement showed the highest rutting values followed by Sections 6 and 2, while the rutting of other sections is less than 0.25 inches.

After the construction, the average rutting values of data collection in June 2019 (after 5 years of service) were 0.04, 0.12, 0.06, 0.05, 0.09 and 0.07 inches respectively for the six sections. These rutting numbers were so small and thus rutting has not been an issue for those sites. Comparing the rutting values before and after SPS-10 construction, it can be concluded that no evident supports that previous pavement condition could affect the after construction pavement performance. In addition, the WMA performs equivalently as compared with to the HMA control section in terms of pavement rutting. This observation is in line with previous research in field performance of WMA technologies (Sargand et al., 2012; West et al., 2014).

3.3 Pavement Roughness

Pavement profile data is automatically collected by the AMES® high speed Profiler at posted speed limit, and the International Roughness Index (IRI) is calculated and summarized at every 25 ft. intervals. The IRI values over time within the two wheel-paths were calculated and averaged for each section, as displayed in Figure 3.16 and Table 3.5.

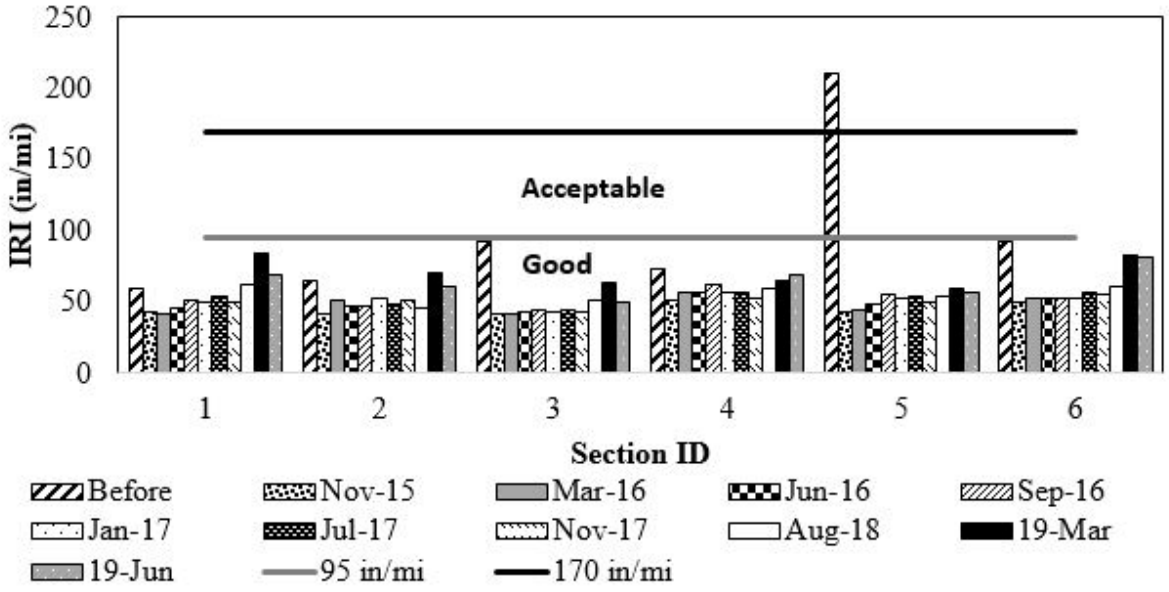

Figure 3.16 IRI Values over Time

Table 3.5 IRI Values of Each Section over Time (in/mi)

Testing Time	Section 1	Section 2	Section 3	Section 4	Section 5	Section 6
Before	59.73	65.42	92.07	73.07	210.78	92.24
Nov-15	42.91	42.16	41.50	51.84	42.51	49.92
Mar-16	41.55	51.25	42.00	57.05	44.01	52.06
Jun-16	46.06	47.78	43.44	56.85	49.02	52.35
Sep-16	50.95	47.42	45.13	62.97	56.01	52.50
Jan-17	49.81	52.23	43.28	56.99	52.12	52.83
Jul-17	54.00	48.38	43.97	57.03	54.04	56.54
Oct-17	50.11	51.70	42.65	53.06	50.56	55.38
Jul-18	62.20	46.16	51.74	59.77	54.54	61.65
Mar-19	84.03	69.99	63.28	64.64	60.27	83.26
Jun-19	69.44	60.86	50.05	68.67	56.48	81.73

Arhin et al. (2015) stated that IRI values ranging from 96 in/mi to 170 in/mi indicate “acceptable” road segments, and IRI less than 95 in/mi are considered to be “good” road segments. On these sections, the average IRI values before

construction were 59.73, 65.42, 92.07, 73.07, 210.78, and 92.24 in/mi respectively. Therefore, before the construction, Section 5 showed the highest IRI values in the “Acceptable” condition, while the other five sections were in “Good” condition in terms of pavement roughness.

After the construction, the average IRI values in June 2019 (after five-years of services) were 69.44, 60.86, 50.05, 68.67, 56.48, and 81.73 in/mi respectively for the six sections. The average IRI numbers have slightly increased since November 2015, but all the sites were still in good conditions with IRI value less than 95 in/mi. Therefore, no distinct difference is perceived in pavement roughness performance among the WMA and HMA technologies thus far. This observation agrees with previous research on field performance of WMA technologies (Sargand et al., 2012). Furthermore, by comparing the IRI numbers before and after SPS-10 construction, no evident supports that previous pavement condition could affect the after construction pavement roughness.

3.4 Pavement Macrotexture

It is widely accepted that surface macrotexture is a predominant contributor to wet-pavement safety. The high-speed pavement macrotexture measurement was performed using the AMES® high-speed profiler. The Mean Profile Depth (MPD) were calculated at every 3.28 ft. (1 m) according to the ASTM Standard E1845-15 (2015) and averaged for each section. The average MPD numbers for each section before and after construction are displayed in Figure 3.17 and summarized in Table 3.6.

On these sections, the average MPD values of data collection before construction were 0.041, 0.042, 0.050, 0.043, 0.043, and 0.039 inches respectively. Before construction, Section 3 showed a higher MPD values than other sections. After the construction, Section 6 exhibited distinguish higher MPD results than other sections. The average MPD values of data collection in June 2019 were 0.039, 0.043, 0.046, 0.044, 0.033, and 0.064 inches respectively for the six sections. Again, no evident supports that previous pavement condition could affect the after construction pavement macrotexture.

Moderate to significant differences were observed between the first two data collection events for most sections, while the trends of MPD values were more consistent during the later eight data collection events. Remaining debris on the pavement surfaces, presence of traffic control safety cones, and the fresh bitumen film in the asphalt mix were the possible reasons that contribute to the variations of MPD measurements in the November 2015 data collection event. Section 6 with SMA mixture maintains the highest texture depth, while Sections 1 to 5 have similar macrotexture properties since they are constructed with the same aggregate gradation.

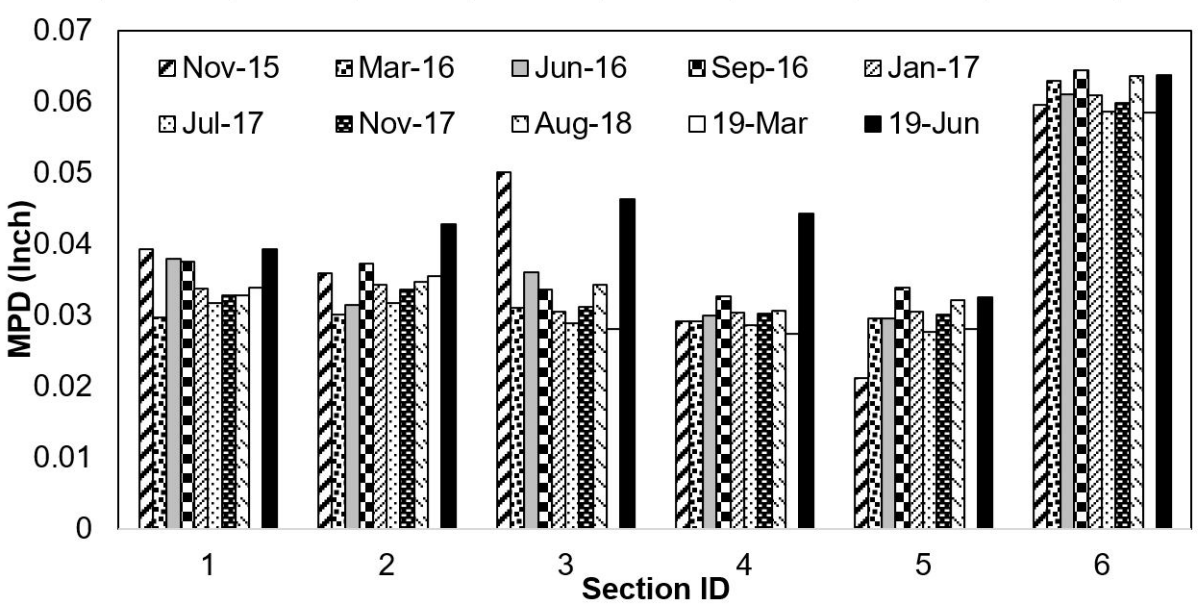

Figure 3.17 MPD Values over Time

Table 3.6 MPD Values, by Section over Time (Inch)

Testing Time	Section 1	Section 2	Section 3	Section 4	Section 5	Section 6
Before	0.041	0.042	0.050	0.043	0.043	0.039
Nov-15	0.039	0.036	0.050	0.029	0.021	0.060
Mar-16	0.030	0.030	0.031	0.029	0.030	0.063
Jun-16	0.038	0.031	0.036	0.030	0.030	0.061
Sep-16	0.038	0.037	0.034	0.033	0.034	0.064
Jan-17	0.034	0.034	0.031	0.030	0.030	0.061
Jul-17	0.032	0.032	0.029	0.029	0.028	0.059
Oct-17	0.033	0.034	0.031	0.030	0.030	0.060
Jul-18	0.033	0.035	0.034	0.031	0.032	0.064
Mar-19	0.034	0.035	0.028	0.027	0.028	0.058
Jun-19	0.039	0.043	0.046	0.044	0.033	0.064

3.5 Pavement Friction

Skid resistance is the ability of the pavement surface to prevent the loss of tire traction. For this project, pavement friction data were collected continuously using the OSU Grip Tester after the construction of SPS-10 to evaluate pavement

skid resistance. The friction number was measured and saved at 3.28 ft. (1 m) intervals. The average friction numbers for each section are displayed in Figure 3.18 and listed in Table 3.7.

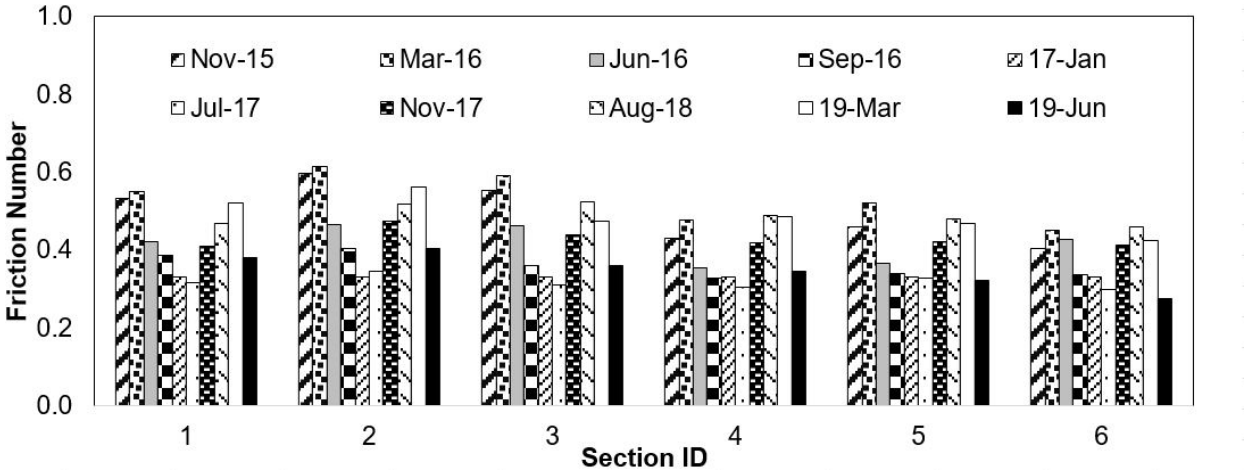

Figure 3.18 Friction Numbers over Time

Table 3.7 Friction Numbers of Each Section over Time

Testing Time	Section 1	Section 2	Section 3	Section 4	Section 5	Section 6
Nov-15	0.53	0.60	0.55	0.43	0.46	0.40
Mar-16	0.55	0.61	0.59	0.48	0.52	0.45
Jun-16	0.42	0.47	0.46	0.35	0.37	0.43
Sep-16	0.39	0.40	0.36	0.33	0.34	0.34
Jan-17	0.33	0.33	0.33	0.33	0.33	0.33
Jul-17	0.31	0.34	0.31	0.30	0.33	0.30
Oct-17	0.41	0.47	0.44	0.42	0.42	0.41
Jul-18	0.47	0.52	0.52	0.49	0.48	0.46
Mar-19	0.52	0.56	0.47	0.48	0.47	0.43
Jun-19	0.38	0.40	0.36	0.34	0.32	0.28
Average	0.43	0.47	0.44	0.40	0.40	0.38

Figure 3.18 illustrates the tendency of friction number over time from November 2015 to June 2019. It is consistent for all the sections that the friction

numbers fluctuate over time while it maintains a friction level around 0.40. For the data collection in June 2019, average friction numbers were 0.38, 0.40, 0.36, 0.34, 0.32, and 0.28 respectively for the six sections. Since Sections 1 to 5 were constructed with the same aggregate gradation, the WMA sections perform equivalently as compared to the HMA control section in terms of pavement friction.

Hall et al. (2009) grouped the influencing factors of pavement friction measurement into four categories: pavement surface characteristics, vehicle operational parameters, tire properties, and environmental factors. Water film depth was one of the most influencing factors for tire-road friction testing (Cerezo et al., 2014; Do et al., 2014). Therefore, the research team conducted an additional special friction testing to investigate the influence of water film depth (0.25 mm and 1.0 mm) on friction measurements. The results are summarized in Figure 3.19 and Table 3.8.

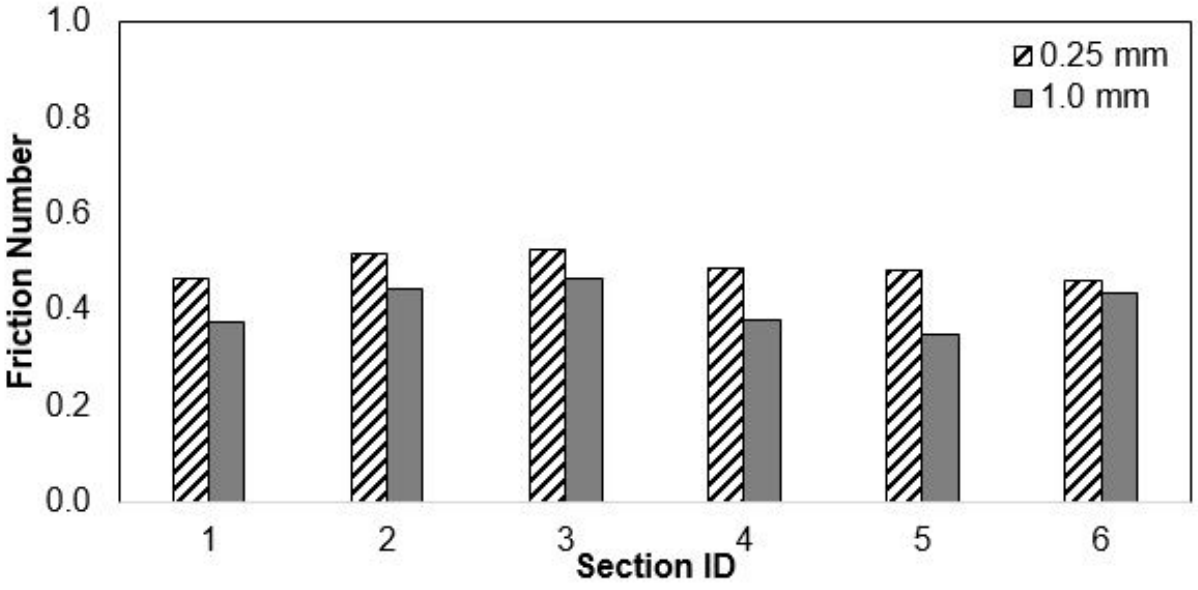

Figure 3.19 Friction Numbers over Time

Table 3.8 Friction Numbers of Each Section from Different Water Film Depths

Water Film Depth (mm)	Section 1	Section 2	Section 3	Section 4	Section 5	Section 6
0.25	0.47	0.52	0.53	0.49	0.48	0.46
1.0	0.38	0.45	0.46	0.38	0.35	0.44
Reduction (%)	19.46	14.03	11.81	22.27	27.42	5.22

At 0.25 mm water film depth, the average friction numbers were 0.47, 0.52, 0.53, 0.49, 0.48, and 0.46 for these sections, respectively. Even Section 6 uses SMA as its gradation design, the obtained friction number under this circumstance was similar to other sections. In other words, Section 6 with SMA mix did not show significant differences in friction resistance as other research claimed (NAPA, 2002).

When the water film depth increased to 1.0 mm, the average friction numbers were 0.38, 0.45, 0.46, 0.38, 0.35, and 0.44 for the six sections, respectively. The friction number of Section 6 with SMA was 0.44 which was higher than other sections. Furthermore, because of the increase in water film depth, 19.46%, 14.03%, 11.81%, 22.27%, 27.42%, and 5.22% of friction reduction was observed for all the six sections respectively. Section 6 with SMA mixture displayed the minimum reduction of friction number (5.22%), which indicated that SMA had a better capability to maintain skid resistance when the water film depth increased.

CHAPTER 4 3D TEXTURE INDICATORS FOR PAVEMENT FRICTION

In this chapter, twenty-four three-dimensional (3D) areal parameters in five categories were implemented to characterize pavement texture attributes and subsequently the relationship among pavement friction and the 3D texture parameters were developed. Pavement texture and friction data were collected in parallel at the same predefined locations via a portable ultra-high resolution 3D laser scanner and a Dynamic Friction Tester (DFT) respectively. Correlation analyses among the 3D texture parameters were conducted to exclude those who exhibit strong correlations and remove the potential multicollinearity for regressional friction model development. Subsequently multivariate analysis was performed to develop the relationship between the selected 3D texture parameters and DFT friction data at various testing speeds. The core material volume and the peak density were identified as the most influential macro- and micro-texture parameters which exhibited fairly good correlation with friction data at high- and low-speed in wet conditions.

4.1 Introduction

4.1.1 Background

Pavement friction is the force resisting the relative motion between the vehicle tire and pavement surface, and pavement texture is defined as the deviations of the pavement surface from a true planar surface (Hall et al., 2009). Pavement friction

can be measured using British Pendulum Tester, Dynamic Friction Tester, Locked-Wheel Skid Trailer, or the Wehner/Schulze equipment statically or dynamically (ASTM E303-93, 2013; ASTM E1911-09a, 2009; ASTM E274/E274M-115, 2015; Do et al., 2007). Pavement macrotexture can be evaluated in terms of mean texture depth (MTD) or mean profile depth (MPD) via sand patch, circular track meter, or high speed profiler (ASTM E965-15, 2015; ASTM E2157-15, 2015; Flintsch et al., 2012). Micro-texture of aggregates or pavement coring samples can be characterized using high resolution devices in the laboratory and evaluated by various methods such as imaging analysis (Dunford et al., 2012; Nataadmadja et al., 2012; Ergun et al., 2005; Ueckermann et al., 2015). It is widely agreed that pavement macro- and micro-texture are the primary contributors to pavement friction performance at high and low traffic speeds (Henry, 2000). However, thus far no consistent relationships have been developed for pavement texture and friction if depending on the widely used traditional texture indicators, such as MPD and MTD (Izeppi et al., 2010).

With the development of non-contact 3-Dimensioal (3D) measurement technologies and the improvement in the computing and processing power of computers in the past decades, it is feasible and desirable to describe road surface texture in both macro- and micro-scale under 3D at high resolution. These 3D based indices and parameters not only promise a quantum leap in describing road surface texture characteristics, but also provide in-depth understanding of the relationship between texture and friction for the purpose of replacing existing costly friction measurement methodologies. Using new texture parameters which are highly

relevant to wet pavement friction could aid in the screening of road network and identifying road segments requiring investigative friction measurements.

Various processing technologies have been applied to analyze 2-Dimensional (2D) or 3D pavement texture profiles for the development of new texture indicators. Wavelet analysis, Hilbert-Huang transform, fractal analysis, and the power spectra density methodology were some of the examples used to characterize pavement macrotexture and relate pavement surface macrotexture attribute to friction performance (Zelelew et al., 2014; Kane et al., 2015; Villani et al., 2014; Hartikainen et al., 2014; Yang et al., 2018). Other studies measured 3D pavement macrotexture data in the field via high-speed laser scanners using a wide range of texture indicators and evaluated their relationships with pavement friction performance (Li et al., 2016; Liu and Shalaby; 2015). There has been limited research to investigate the relationship between pavement friction and micro-texture based on 2D pavement profiles or 3D images with resolution up to 0.015 mm; however, they relied on traditional texture parameters and failed to identify the proper texture parameters to predict pavement friction performance (Serigos, 2013; Li et al., 2016; Kanafi et al., 2015; Bitelli et al., 2012). Therefore, understanding the relationship between macro- and/or micro-texture and friction performance under 3D conditions using proper 3D texture parameters deserves further research.

In this chapter, a wide variety of 3D areal surface parameters were investigated. The first group of parameters is calculated by taking every data point measured on a 3D areal surface into account, while the second group only considers specific points, lines or areas which are identified as features such as peaks and

valleys (Leach, 2012). Other parameters can be further categorized into height parameters, function related parameters, hybrid parameters, and spatial parameters; while feature parameters generally contain peak density, peak curvature, motif slope, significant heights, and morphological parameters (Leach, 2012). According to the definition in ASTM E1845-15 (26), the currently widely used macrotexture parameters, MPD and MTD, belong to the height parameter family and only reflect one attribute of the pavement surface texture. It is necessary to perform a comprehensive evaluation of pavement texture via various available 3D areal parameters, and investigate their contributions to pavement friction performance at both macro- and micro-levels.

4.1.2 Objective

The objective of this chapter is to identify proper 3D areal texture parameters with good representation to friction performance, and develop corresponding pavement friction prediction models based on the selected 3D areal texture parameters. The LTPP SPS-10 testing site in Oklahoma, including six warm-mix-asphalt (WMA) sections, was selected as the field testing bed. Pavement friction and texture data were collected via a Dynamic Friction Tester (DFT) and a portable 3D laser scanner with ultra-high resolution up to 0.05 mm and 0.01 mm in the lateral and the vertical directions, respectively. Twenty-four 3D areal parameters covering all categories of available texture indicators were calculated for each 3D measurement.

Correlation analyses of those 3D parameters were conducted to exclude those who exhibit strong correlations and remove the potential multicollinearity for

regressional friction model development. Subsequently multivariate analysis was performed to develop the relationship between the selected 3D texture parameters and DFT friction data at different testing speeds.

4.2 Testing Devices

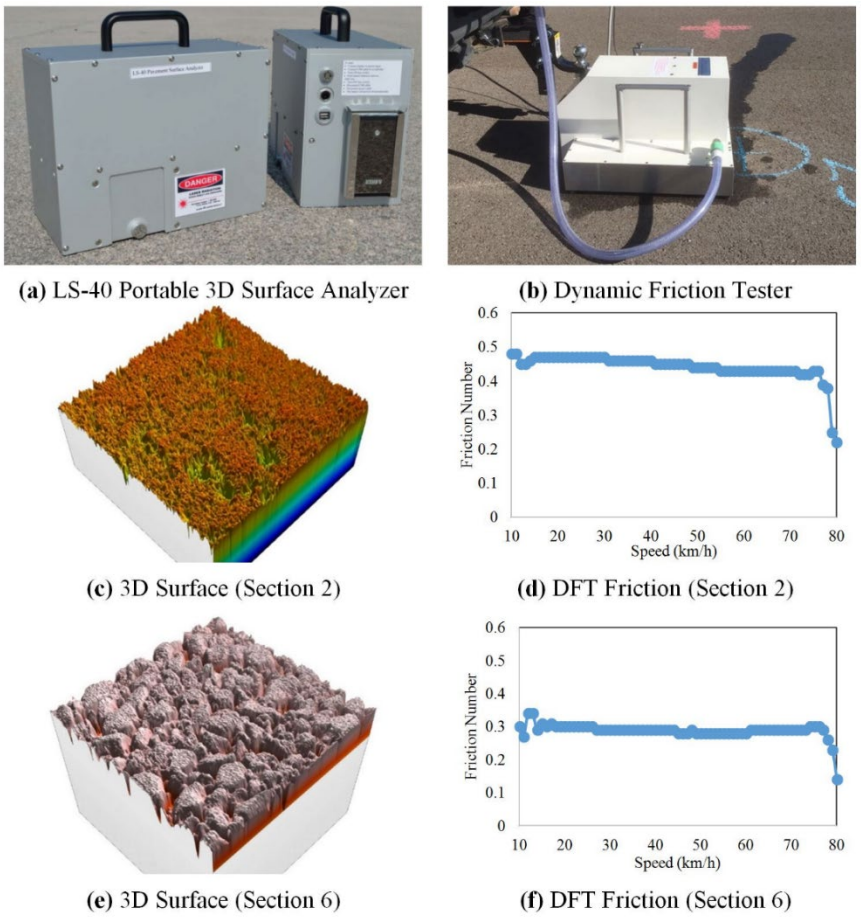

Figure 4.1 Data Collection Devices and Example Data Sets

4.2.1 LS-40 Portable 3D Surface Analyzer

A 3D surface measurement and analysis device, named LS-40 Portable 3D Surface Analyzer (Figure 4.1.a) (LS-40 for short), scans a 4.5” by 4” pavement surface and collects 3D texture data with height resolution (z) at 0.01 mm and lateral resolution (x, y) at 0.05 mm. LS-40 provides 3D surface data to calculate MPD by

processing thousands of profiles over the entire scanned surface according to ASTM E1845 (2015) specifications, with optional processing modules of measuring other surface features, such as aggregate form factor, angularity calculation based on multiple contour measurements, and micro-texture indicators, such as Root Mean Square (RMS). LS-40 can not only be used in the laboratory, but also be placed on a localized pavement surface area in the field to collect 2048 by 2448 cloud points for pavement texture characterization. Figures 4.1.c and 4.1.e are two example 3D pavement data collected on Section 2 and 6 respectively.

4.2.2 Dynamic Friction Tester

ASTM E1911-09a (2009) provides specification on measuring paved surface frictional properties using the Dynamic Friction Tester (DFT). A DFT (Figure 4.1.b) consists of a horizontal spinning disk fitted with three spring loaded rubber sliders. The water is sprayed in front of the sliders and a constant load is applied to the slider as the disk rotating on the test surface. The torque is monitored continuously as the disk rotational velocity reduces due to the friction between the sliders and the test surface, then it is used to calculate the surface friction coefficients. DFT has been widely used in friction measurement under various conditions to explore the speed dependency of pavement friction by measuring friction at various speeds. Figures 4.1.d and 4.1.f are two example DFT friction data measured at the same locations where texture data were collected as demonstrated in Figures 4.1.c and 4.1.e.

4.3 Preliminary Results

The data collection efforts described herein included two data collection activities, the first on November 13th, 2015 immediately after the construction of the testing site and the second on May 25th 2016 when the Sections were approximately 6-month in age, on the six LTPP SPS-10 Sections and the transition sections in-between. LS-40 Portable 3D Surface Analyzer and DFT were used to measure pavement 3D surface data and friction data separately in the right wheelpath (approximately 3.0 ft. from the shoulder) in parallel at the same predefined locations. Within each LTPP SPS-10 section, three pairs of LS-40 3D data and DFT friction data were obtained at 100 ft. interval starting from the beginning of the section. As the mainline after each LTPP SPS-10 section, another three pairs of pavement texture and friction measurement were conducted at 300 ft interval from the ending of the section. Therefore, thirty-six pairs of pavement 3D texture and friction data measurement were obtained for each data collection. Finally, sixty-nine pairs of pavement texture and friction data were analyzed after three data sets were removed due to the bad data quality.

For preliminary analysis, MPD for each 3D measurement was calculated, while pavement DFT friction numbers at various testing speeds from 10 km/h to 70 km/h were produced. The average DFT friction numbers at speeds from 10 km/h to 70 km/h and the average MPD for each SPS-10 section and transition were plotted in Figure 4.2. The column labels in the figure are for Section 1, Transition 1, Section 2, Transition 2, …, Section 6, Transition 6 from left to right.

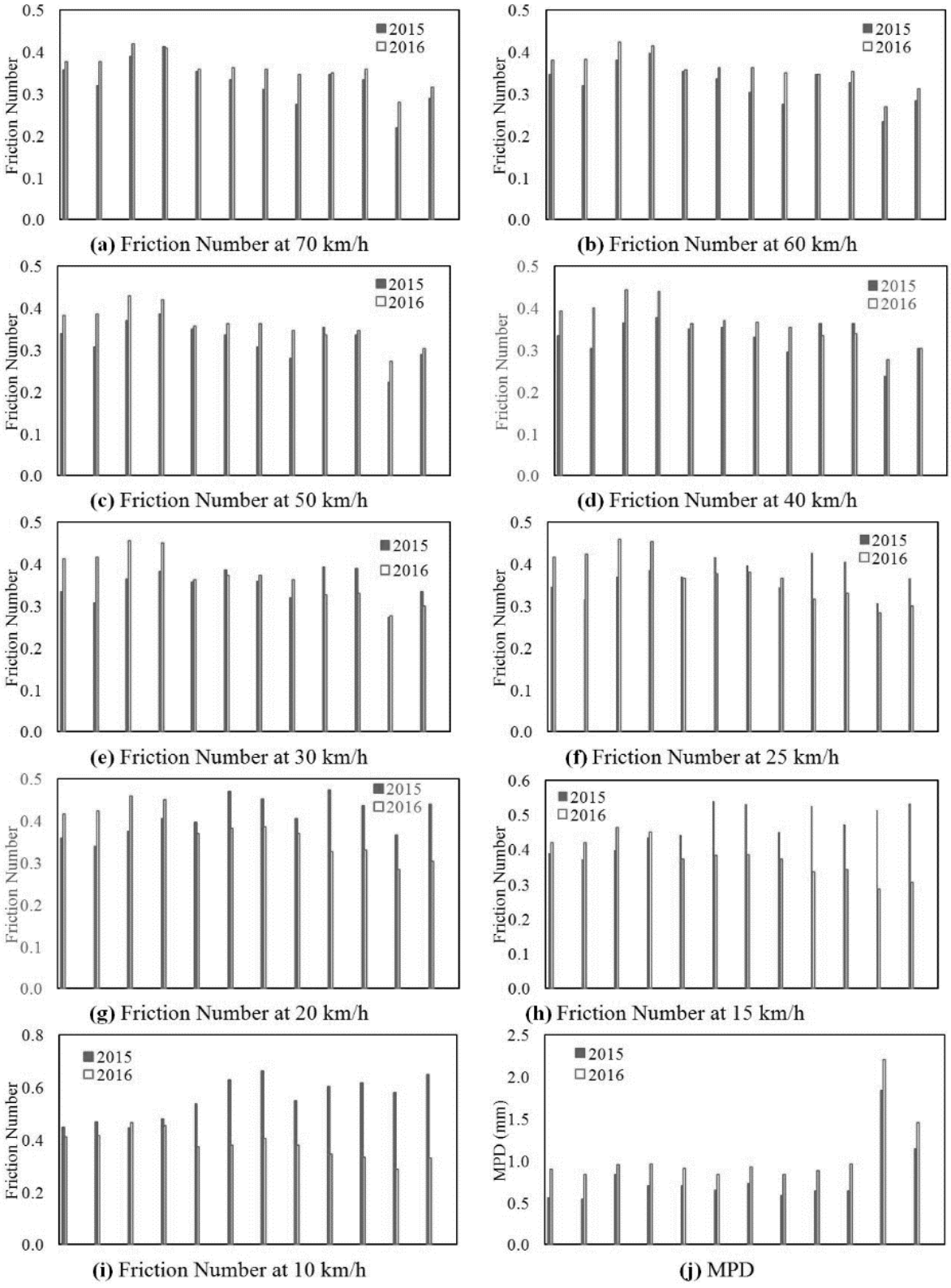

Figure 4.2 Average DFT Friction at Various Testing Speeds and MPD

It is illustrated that the average friction numbers at speeds over 40 km/h show an increase tendency between the two data collection events (Figures 4.2.a through 4.2.d), whereas the average friction numbers at speeds lower than 20 km/h exhibit a decrease tendency for most of the locations (Figures 4.2.g to 4.2.i). For example, the average friction numbers at 60 km/h for Sections 1 through 6 are 0.35, 0.38, 0.35, 0.30, 0.35, and 0.23 for the first data collection in 2015, and 0.38, 0.42, 0.36, 0.36, 0.34 and 0.27 for the second collection in 2016. The average friction numbers at 10 km/h for Sections 1 through 6 are 0.45, 0.45, 0.54, 0.66, 0.60, and 0.58 in 2015, while 0.41, 0.47, 0.37, 0.41, 0.35 and 0.29 in 2016. At speeds from 20 km/h to 30 km/h (Figures 4.2.e to 4.2.g), no consistent tendency is observed on these sections. On the other hand, the average MPD values for each of the six SPS-10 section and transition section display an increasing tendency, as shown in Figure 4.2.j. The average MPD for Sections 1 through 6 are 0.56 mm, 0.84 mm, 0.71 mm, 0.73 mm, 0.64 mm, and 1.84 mm in 2015, and 0.90 mm, 0.95 mm, 0.91 mm, 0.93 mm, 0.88 mm and 2.21 mm in 2016.

Generally, the evolution of skid resistance with an initial increase in friction coefficient occurs in the following months immediately after the laying of the road surface. Due to the applications of traffic polish, the bitumen film which masks the aggregate is gradually removed and the pavement friction number gradually increases. During the binder removal phase, more aggregates are exposed to the pavement surface. The binder removal period could range from 6 months to 2 years (Do et al., 2007). Since 60 km/h is the standard testing speed to collect friction number (ASTM E1911-09a, 2009), it is logical that the friction numbers have

increased over the last 6-month as shown in Figure 4.2.b. In addition, “new” surface texture may be generated under potential “differential” traffic polishing (Nataadmadja et al., 2012), which probably results in the increase of the average MPD values during the last 6-month period.

On the other hand, Section 6 shows distinct higher average MPD values comparing to those on the other sections for both data collections (Figure 4.2.j), while the average DFT friction numbers on Section 6 are relatively lower for testing speeds over 25 km/h (Figures 4.2.a to 4.2.f). The relatively lower insoluble residue value of the aggregates (Table 2.1) and the observed thick bitumen film after construction are the possible reasons for the lower skid resistance of Section 6. In addition, friction and MPD data on Section 6 show opposite development tendency for both collection events at speeds lower than 20 km/h (Figures 4.2.g to 4.2.j). Since MPD fails to capture the differences and variations in friction performance both at high and low speeds, new texture parameters are needed to be developed to relate pavement texture with friction performance at macro- and micro-level.

4.4 3D Areal Texture Parameters

After a thorough literature review, there are five different categories of 3D areal parameters used in various areas: height parameters, volume parameters, hybrid parameters, spatial parameters, and feature parameters, all of which are calculated and used to relate pavement texture characteristics to friction performance in this study. The first four categories of parameters are generally classified as field parameters which are calculated using all the data point measured in a 3D surface. The last category is calculated based upon the features which play

specific role in a particular function on a 3D image. For each category, several different texture parameters are used for various purposes. The definitions of the 3D areal parameters and their calculations for each category are provided in the following sections.

4.4.1 Height Parameters

The arithmetic mean height (Sa), the root mean square height (Sq), the skewness (Ssk), the Kurtosis (Sku), the maximum height of the surface (Sp, Sv, and Sz), and the traditional mean profile depth (MPD) are typical height texture parameters. Sp is the maximum peak height, Sv is the maximum pit height, and Sz is the maximum height of the surface (Leach, 2012). The definitions of Sa, Sq, Ssk, and Sku are shown in Equations 4.1 to 4.4 individually. In the equations the function z(x,y) is the height of a pixel in mm at location (x,y) within the 3D image and A is the sampling area (Leach, 2012).

$$S_a = \frac{1}{A}\iint_A z(x,y)\,dx\,dy \tag{4.1}$$

$$S_q = \sqrt{\frac{1}{A}\iint_A z^2(x,y)\,dx\,dy} \tag{4.2}$$

$$S_{sk} = \frac{1}{{S_q}^3}\frac{1}{A}\iint_A z^3(x,y)\,dx\,dy \tag{4.3}$$

$$Sk_u = \frac{1}{{S_q}^4}\frac{1}{A}\iint_A z^4(x,y)\,dx\,dy \tag{4.4}$$

The calculation of MPD is defined in ASTM E1845-15 (2015), which only considers the average height of the two highest peaks of two 50 mm profile segments. Sa is generally used to capture the roughness variation of road surfaces under traffic wear in laboratory (Dunford et al., 2012). Sa and Sq are insensitive in differentiating peaks, valleys and the spacing of the various texture features, thus pavement surfaces with same Sa or Sq may function quite differently (Michigan Metrology, 2014).

4.4.2 Volume Parameters

The volume parameters, including the void volume (Vv), the material volume (Vm), the peak material volume (Vmp), the core material volume (Vmc), the core void volume (Vvc) and the dales void volume (Vvv), are function related parameters (Leach, 2012; Michigan Metrology, 2014). The material ratio (mr), defined in Figure 4.3.a, is the ratio in percentage of the length of bearing surface at any specified depth in a profile (Michigan Metrology, 2014). mr simulates surface wear of a 3D pavement surface which provides a bearing surface for vehicle tires. As the cutting plane moves down from the highest peak to the lowest valley of a profile, mr will increase along with the bearing surface and range up to 100%. The areal material ratio curve (the dashed line as shown in Figure 4.3.b) is the cumulative curve of mr from the highest peak to the lowest valley (Michigan Metrology, 2014).

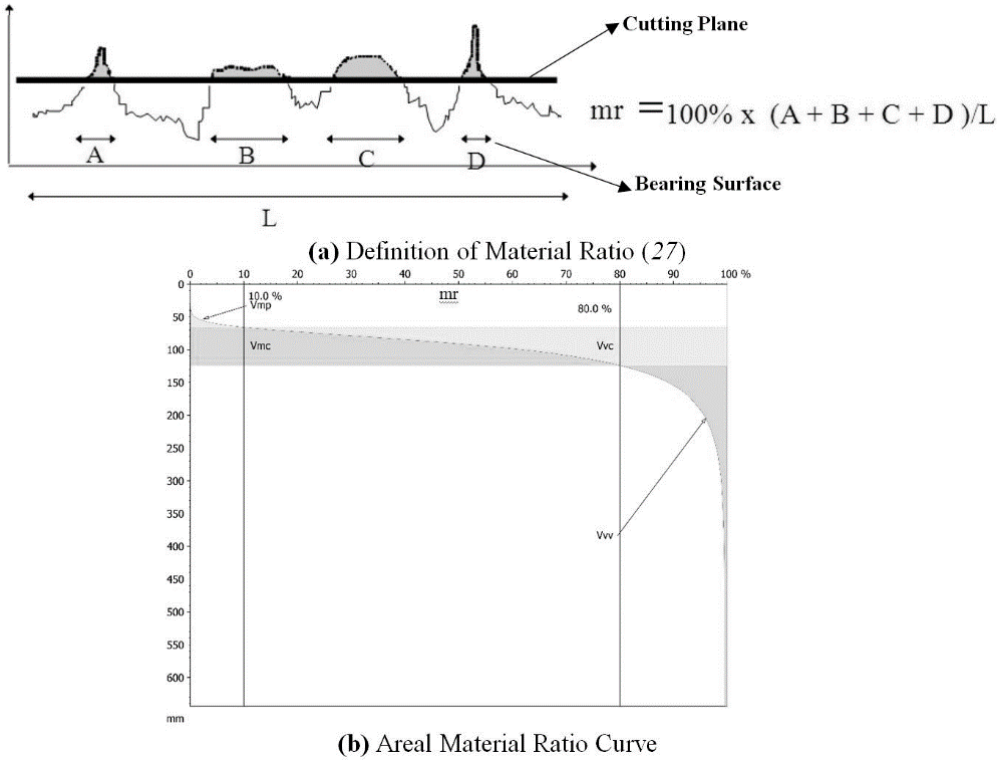

Figure 4.3 Calculation of Volume Parameters

Vv (Vm) for a material ratio mr is calculated by integrating the volume enclosed above (below) the 3D texture image and below (above) the horizontal cutting plane at the height corresponding to mr (Leach, 2012). Vvc (Vmc) is defined as the difference between two void (material) volume values calculated at different heights corresponding to mr1 and mr2, while Vvv (Vmp) is defined as the void (material) volume calculated at the height corresponding to mr2 (mr1).

$$V_{vc} = V_v(mr1) - V_v(mr2) \tag{4.5}$$

$$V_{mc} = V_m(mr2) - V_m(mr1) \tag{4.6}$$

$$V_{vv} = V_v(mr2) \tag{4.7}$$

$$V_{mp} = V_m(mr1) \tag{4.8}$$

Where mr1 = 10%, mr2 = 80%, and the unit of volume parameters is mm^3/mm^2 herein (Leach, 2012). In Figure 4.3.b, Vvc (Vmc) is the area enclosed above (below) the areal material ratio curve and between the heights corresponding to mr1 and mr2, and Vvv (Vmp) is the area enclosed above (below) the areal material ratio curve and between the height corresponding to mr2 (mr1). The volume parameters can characterize wear and rolling properties during a running-in procedure (Deltombe et al., 2011; Adelle, 2006). Vmc is useful to understand how much material is available for load support once the top levels of a surfaces are worn away (Michigan Metrology, 2014).

4.4.3 Hybrid Parameters

The hybrid parameters are useful to consider both the height and spacing information of a 3D image simultaneously to evaluate texture characteristic (Li et al., 2016). The root mean square gradient (Sdq) and developed interfacial area ratio (Sdr) are defined as Equation 3 and considered herein to differentiate the surface with similar degree of roughness (Leach, 2012; Michigan Metrology, 2014). Sdq and Sdr are affected both by texture amplitude and spacing: a surface with same roughness and wider spaced texture may induce a lower value of Sdq or Sdr (Michigan Metrology, 2014).

$$S_{dq} = \sqrt{\frac{1}{A}\iint \left(\frac{\partial z^2}{\partial x} + \frac{\partial z^2}{\partial y}\right) dxdy} \tag{4.9}$$

$$S_{dr} = \frac{(Texture\_Surface\_Area) - (Cross\_Sectional\_Area)}{Cross\_Sectional\_Area} \tag{4.10}$$

4.4.4 Spatial Parameters

The calculation of spatial parameters involves the understanding of the autocorrelation function (ACF) which evaluates the correlation of the original surface and the duplicated surface with a relatively shift (Dx, Dy) (Leach, 2012; Michigan Metrology, 2014). The autocorrelation length (Sal) defines the distance over the surface such that the new location will have minimal correlation with the original location, and the texture aspect ratio (Str) is the division of the Sal and the length of slowest decay ACF in any direction (Michigan Metrology, 2014). The texture direction (Std), with values between 0º and 180º, is also included to identify the angular direction of the dominant lay comprising a surface (Leach, 2012; Michigan Metrology, 2014). Str can be applied to evaluate surface texture isotropy, and Sal may find application related to the interaction of electromagnetic radiation with the surface and also tribological characteristics such as friction and wear (Leach, 2012; Michigan Metrology, 2014).

4.4.5 Feature Parameters

The feature parameters herein consider the peak density (Spd), the peak curvature (Spc), and the significant height (S5p, S5v, and S10z). A surface point higher than its surrounding area is called a peak, and the significant peaks on a surface are segmented by inverting the surface and applying the watershed segmentation algorithm and the pruning of the change tree by a specified pruning factor (Leach, 2012). Spd and Spc are defined in Equation 4.11 and 4.12 with unites of $1/mm^2$ and 1/mm respectively (Leach, 2012; Michigan Metrology, 2014). S5p

(S5v) is the arithmetic mean height of the five highest (lowest) significant peaks (pits), and S10z is simply the sum of S5p and S5v with unit of mm (Leach, 2012).

Spd can be used in applications where contact is involved along with other parameters, and the peak density can be used to quantify aggregate micro-texture with respect to wear in laboratory (Nataadmadja et al., 2012; Leach, 2012). Spc is useful in predicting the degree of elastic and plastic deformation of a surface under different loading conditions and thus may be used in predicting friction, wear and real area of contact for thermal/electrical applications (Michigan Metrology, 2014). The curvature of a profile was able to quantify aggregate micro-texture with respect to the surface friction under wear condition in laboratory (Nataadmadja et al., 2012)

$$S_{pd} = \frac{Number\ of\ peaks}{Area} \tag{4.11}$$

$$S_{pc} = \frac{1}{N} \iint_{peak-Area} \left(\frac{\partial^2 z(x,y)}{\partial x^2}\right) + \left(\frac{\partial^2 z(x,y)}{\partial y^2}\right) dx\, dy \tag{4.12}$$

4.5 Selection of 3D Texture Parameters

4.5.1 Correlation Analysis

Considering all five categories of 3D areal parameters aforementioned, there are twenty-four different parameters available to represent the 3D texture characteristics of a pavement surface. The calculation of those parameters were calculated via the Mountains® software. The correlation analysis was conducted within each category and among different categories to remove the parameters who exhibited strong correlations and removed their potential multicollinearity for regressional friction model development. Correlation coefficient of 0 means that there is no correlation, -1 denotes a perfect negative correlation, while +1 suggests a

perfect positive correlation between the two variables. A correlation greater than 0.8 is generally described as strong, whereas a correlation less than 0.5 is generally described as weak.

4.5.2 Correlations within Each Category

The correlation coefficients within each category are summarized in Tables 4.1a to 4.1.c.

- Based on Table 4.1, Sq and Ssk are kept to represent as the height parameters since their correlation coefficients with other parameters are less than 0.5. The traditional texture indicator MPD is excluded herein because it is highly correlated with many height parameters such as Sq, Sp, Sv, Sz, and Sa.
- Based on Table 4.2, only Vmc is kept as the volume parameter, and Sdq is selected as the hybrid parameter to evaluate the friction performance between the vehicle tire and the pavement surface.
- Based on Table 4.3, Sal and Str are selected as the spatial parameters while Spd, Spc and S5v are selected as feature parameters due to their lower correlation coefficients with other parameters.

In summary, after the correlation analysis within each texture parameter category, only Sq, Ssk, Vmc, Sdq, Sal, Str, Spd, Spc and S5v are determined as the potential 3D areal parameters, which are not highly correlated within each category, for the development of relationship between pavement texture and friction performance.

4.5.3 Correlations among Categories

Subsequently, correlation analysis among different categories was performed for the previously identified 3D parameters within each category, since correlations may be strong among the parameters within different categories. As shown in Table 4.4, Sq, Sdq, Str, Spc, and S5v are excluded because their correlation coefficients with other parameters are larger than 0.5. Correspondingly, Ssk, Vmc, Sal and Spd, which represents the height, volume, spatial and feature attributes of a 3D surface respectively, are selected as the final list of the 3D areal parameters for friction model development. The statistics of the selected 3D areal parameters on each SPS-10 section and transition are plotted in Figure 4.4 to evaluate the variations of these texture indicators between these two data collection events:

- Vmc and Spd demonstrate decreasing tendency with traffic polish for most locations (Figures 4.4.b and 4.4.c), while Ssk and Sal exhibit inconsistent tendency (Figures 4.4.a and 4.4.d).
- As can be seen in Figure 4.4.c and Figure 4.2.i, the development of Spd corresponds well to the variation tendency of DFT friction number at the speed of 10 km/h.
- On the other hand, because Vmc represents the part of the surface material which does not interact with another surface in contact (Leach, 2012), the smaller the Vmc value, the more surface materials are involved in the contact process with vehicle tires. Therefore, it is observed from Figure 4.4.b and Figures 4.2.a and 4.2.b that the development of Vmc

corresponds well to the variation tendency of friction number at speeds over 60 km/h for all the sections.

Table 4.1 Correlation Analyses of 3D Height Parameters

Parameter	**Sq**	**Ssk**	Sku	Sp	Sv	Sz	Sa	MPD
Sq	1.0	-0.2	0.3	0.9	0.9	1.0	1.0	0.9
Ssk	-0.2	1.0	-1.0	-0.3	-0.2	-0.1	-0.1	-0.2
Sku	0.3	-1.0	1.0	0.4	0.3	0.2	0.2	0.3
Sp	0.9	-0.3	0.4	1.0	1.0	0.9	0.9	0.9
Sv	0.9	-0.2	0.3	1.0	1.0	0.9	0.9	0.9
Sz	1.0	-0.1	0.2	0.9	0.9	1.0	1.0	0.9
Sa	1.0	-0.1	0.2	0.9	0.9	1.0	1.0	0.9
MPD	0.9	-0.2	0.3	0.9	0.9	0.9	0.9	1.0

Table 4.2 Correlation Analyses of 3D Volume and Hybrid Parameters

Parameter	Vm	Vv	Vmp	**Vmc**	Vvc	Vvv	**Sdq**	Sdr
Vm	1.0	0.7	1.0	0.7	0.7	0.6	-	-
Vv	0.7	1.0	0.7	1.0	1.0	1.0	-	-
Vmp	1.0	0.7	1.0	0.7	0.7	0.6	-	-
Vmc	0.7	1.0	0.7	1.0	1.0	0.9	-	-
Vvc	0.7	1.0	0.7	1.0	1.0	0.9	-	-
Vvv	0.6	1.0	0.6	0.9	0.9	1.0	-	-
Sdq	-	-	-	-	-	-	1.0	0.8
Sdr	-	-	-	-	-	-	0.8	1.0

Table 4.3 Correlation Analyses of 3D Spatial and Feature Parameters

Parameter	**Sal**	**Str**	Std	**Spd**	**Spc**	S10z	S5p	**S5v**
Sal	1.0	-0.3	-0.1	-	-	-	-	-
Str	-0.3	1.0	0.5	-	-	-	-	-
Std	-0.1	0.5	1.0	-	-	-	-	-
Spd	-	-	-	1.0	-0.3	-0.3	-0.3	-0.3
Spc	-	-	-	-0.3	1.0	0.9	0.8	0.9
S10z	-	-	-	-0.3	0.9	1.0	0.9	0.9
S5p	-	-	-	-0.3	0.8	0.9	1.0	0.6
S5v	-	-	-	-0.3	0.9	0.9	0.6	1.0

Table 4.4 Correlation Analyses of 3D Areal Texture Parameters

Parameter	Sq	**Ssk**	**Vmc**	Sdq	**Sal**	Str	**Spd**	Spc	S5v
Sq	1.0	-0.2	1.0	0.7	-0.1	0.6	-0.3	0.8	0.8
Ssk	-0.2	1.0	0.0	0.2	0.2	0.2	0.4	0.1	-0.0
Vmc	1.0	0.0	1.0	0.7	-0.1	0.6	-0.3	0.9	0.9
Sdq	0.7	0.2	0.7	1.0	-0.0	0.4	-0.1	0.8	0.7
Sal	-0.0	0.2	-0.1	-0.0	1.0	-0.3	-0.1	-0.1	-0.1
Str	0.6	0.2	0.6	0.4	-0.3	1.0	-0.1	0.5	0.5
Spd	-0.3	0.4	-0.3	-0.1	-0.1	-0.1	1.0	-0.3	-0.3
Spc	0.8	0.1	0.9	0.8	-0.1	0.5	-0.3	1.0	0.9
S5v	0.8	-0.0	0.9	0.7	-0.1	0.5	-0.3	0.9	1.0

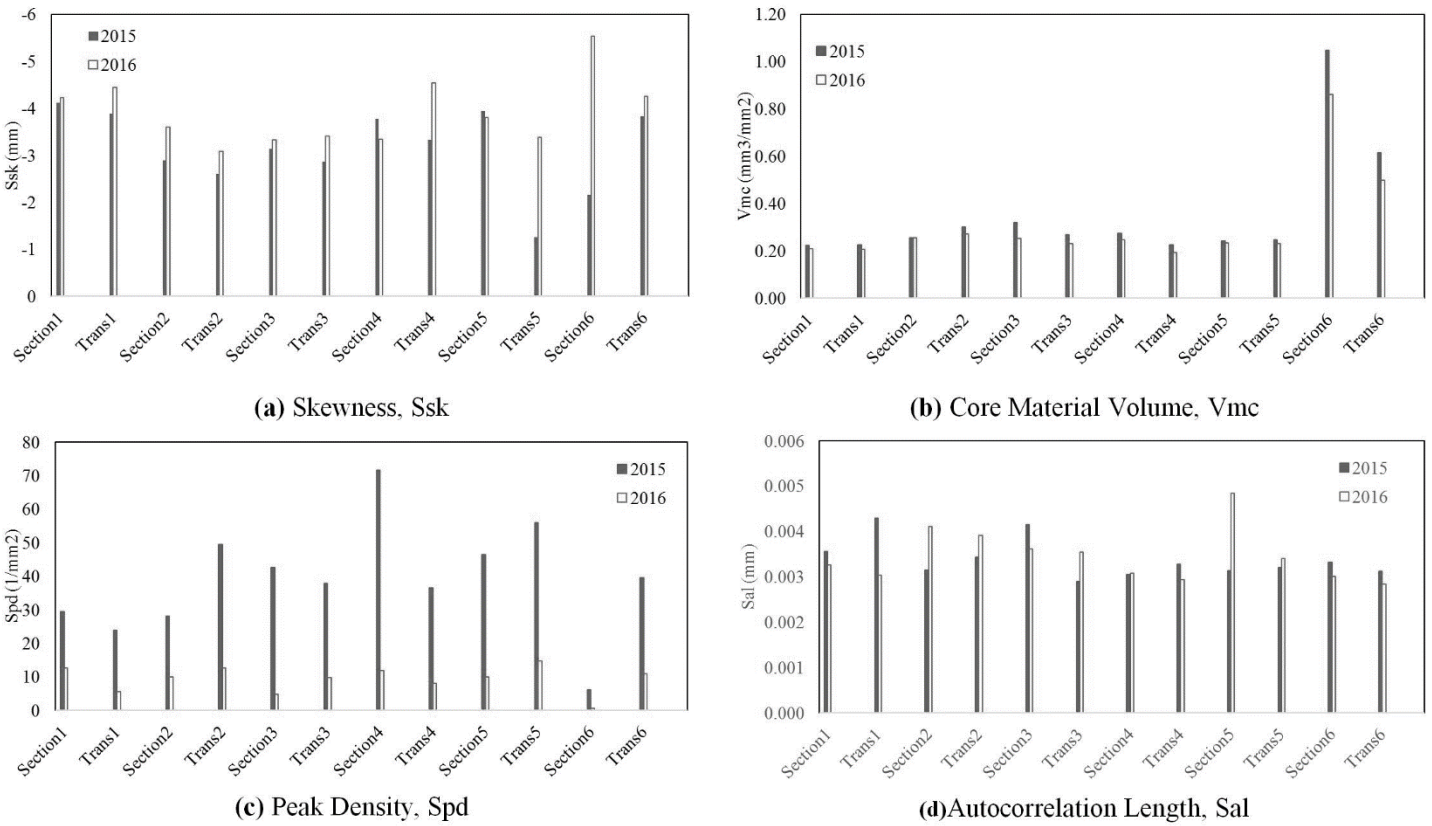

(a) Skewness, Ssk

(b) Core Material Volume, Vmc

(c) Peak Density, Spd

(d) Autocorrelation Length, Sal

Figure 4.4 Comparisons of Selected 3D Pavement Texture Parameters

4.6 Friction Prediction Models

4.6.1 Model Development

The sixty-nine sets of DFT friction numbers at different speeds along with the selected 3D texture parameters, Ssk, Vmc, Sal and Spd, were prepared for model development. Every other data sets were used to develop the friction prediction model at different speeds, while the remaining data sets were reserved for model validation. Multivariate linear regression was conducted to identify the significant confidence level of the selected 3D areal texture parameters on friction number at different speeds. The statistical analysis results are summarized in Table 4.5.

- Vmc and Spd show consistently significant influence on friction numbers for testing speeds over 25 km/h and less than 20 km/h, individually.
- Ssk is identified as a significant parameter for DFT friction tested at speed of 10 km/h only.
- Sal is not a significant factor on friction at any speeds among these selected four parameters.

Table 4.5 Significance of Selected 3D Texture Parameters on DFT Friction at Different Speeds

3D Parameters	DFT70	DFT60	DFT50	DFT40	DFT30	DFT25	DFT20	DFT15	DFT10
Ssk	-	-	-	-	-	-	-	*	*
Vmc	**	**	**	**	**	*	-	-	*
Sal	-	-	-	-	-	-	-	-	-
Spd	-	-	-	-	-	-	*	**	***

Note:
DFTxx means the DFT friction number collected at speed xx km/h; Significance codes: '***' $p < 0.001$, '**' $p < 0.01$, '*' $p < 0.05$, '-' $p > 0.05$. For example '*' indicates the P-value is less than 0.05 and the parameter is significant to the friction number; '-' means the P-value is larger than 0.05 and the parameter is not significant to the friction number.

Subsequently, friction prediction models were developed based on only the significant 3D areal parameters at different speeds. The estimated regression coefficients and P-values of friction prediction models are summarized in Table 4.6 and Table 4.7. The sample number is 34. All the P-values for the 3D areal texture parameter herein are smaller than 0.05 in the proposed model, indicating their significance to pavement friction. Therefore, the friction number at different speeds are valid and can be calculated based on the selected 3D areal parameters as Equation 4.13:

$$Friction\ Number = a + \sum_1^3 \mathrm{T}_i * b_i \tag{4.13}$$

Where a is the estimated coefficient for intercept, Ti represents the Vmc, Ssk and Spd of a 3D pavement surface, and bi is the estimated coefficient for the corresponding 3D areal parameter at different speeds.

Table 4.6 Statistic Results of Friction Prediction Models based on Selected 3D Areal Texture Parameters

DFT Friction at Speed (km/h)	Item	Coefficient	P-value	Validation R^2	Validation SSE
70	Intercept	0.395	6.36E-26	0.58	0.031
70	Vmc	-0.138	8.07E-05	0.58	0.031
60	Intercept	0.394	7.58E-26	0.57	0.034
60	Vmc	-0.144	4.54E-05	0.57	0.034
50	Intercept	0.391	4.38E-26	0.54	0.038
50	Vmc	-0.136	7.63E-05	0.54	0.038
40	Intercept	0.394	3.83E-26	0.48	0.044
40	Vmc	-0.127	0.00018	0.48	0.044
30	Intercept	0.399	2.74E-25	0.37	0.057
30	Vmc	-0.110	0.001804	0.37	0.057
25	Intercept	0.405	1.16E-24	0.29	0.066
25	Vmc	-0.091	0.012268	0.29	0.066
20	Intercept	0.362	2.81E-23	0.33	0.089
20	Spd	0.001	0.003921	0.33	0.089
15	Intercept	0.368	5.68E-21	0.38	0.131
15	Spd	0.002	8.28E-05	0.38	0.131
10	Intercept	0.414	1.63E-07	0.54	0.209
10	Ssk	0.027	0.043722	0.54	0.209
10	Vmc	0.181	0.002568	0.54	0.209
10	Spd	0.004	3.21E-06	0.54	0.209

Table 4.7 Statistic Results of Friction Prediction Models based on MPD

DFT Friction at Speed (km/h)	Item	Coefficient	P-value	Validation R^2	Validation SSE
70	Intercept	0.401	2.44E-20	0.30	0.051
70	MPD	-0.055	5.52E-03	0.30	0.051
60	Intercept	0.399	4.80E-20	0.29	0.055
60	MPD	-0.056	5.15E-03	0.29	0.055
50	Intercept	0.397	1.91E-20	0.26	0.060
50	MPD	-0.054	5.76E-03	0.26	0.060
40	Intercept	0.399	1.09E-20	0.25	0.063
40	MPD	-0.050	0.00832	0.25	0.063
30	Intercept	0.407	1.06E-20	0.26	0.067
30	MPD	-0.048	0.01288	0.26	0.067
25	Intercept	0.420	5.22E-21	0.26	0.069
25	MPD	-0.048	0.01302	0.26	0.069
20	Intercept	0.441	5.12E-20	0.21	0.097
20	MPD	-0.048	0.02860	0.21	0.097
15	Intercept	0.473	1.29E-16	0.10	0.192
15	MPD	-0.048	0.10751	0.10	0.192
10	Intercept	0.531	6.87E-13	0.16	0.373
10	MPD	-0.061	0.18092	0.16	0.373

4.6.2 Model Validation

Based on Equation 4.13, the predicted friction numbers of the validation data sets were calculated and compared with the actual friction numbers to validate the proposed models. The validation results of the developed friction prediction model at different speeds are also summarized in Table 4.6. The R-squared values are 0.54 to 0.58 between the predicted and the actual DFT friction numbers at speeds from 10 km/h to 70 km/h, respectively. Generally speaking, the friction prediction models at higher testing speeds have better performance than those at lower speeds. The sum of squared error (SSE) for the proposed models at speed 70 km/h to 10 km/h

increases from 0.031 to 0.209. Example of the actual and the predicted friction numbers at high and low speeds are compared in Figures 4.5.a and 4.5.b.

To demonstrate the advantages of the proposed parameters, linear regression friction prediction models at different testing speeds were also developed considering MPD as the influencing texture parameter. The estimated regression coefficients and P-values are also provided in Table 4.7. The P-values for the MPD based models are smaller than 0.05 for testing speeds over 20 km/h, indicating the significance of MPD to pavement friction at high speed. However, the P-values are greater than 0.05 for models at the testing speeds of 15 km/h and 10 km/h, indicating the insignificance of MPD to pavement friction at low speed. The R-squared values of the MPD based models range from 0.1 to 0.3 between the predicted and actual DFT friction numbers, which are much lower than those for the proposed models based on the 3D texture indicators. In addition, the sum of squared errors of prediction (SSE) in the MPD based model are consistently higher than those in the models from this paper, proving that the DFT friction models based on the selected 3D areal texture parameters are more robust. Examples of the actual and the predicted friction numbers at high and low speeds are compared in Figures 4.5.c and 4.5.d.

Based on Tables 4.5 and 4.6, Vmc is the only significant parameter on friction number for the models at speeds over 20 km/h, whereas the Spd is the only significant parameter on friction number for the models at speeds 20 km/h and 15 km/h. Even though there are three significant parameters in the model at 10 km/h, Spd is the dominate parameter over the other two based on their P-values.

Therefore, it can be concluded that Vmc and Spd are the 3D areal parameters corresponding to macro- and micro-texture for friction prediction at high (over 40 km/h) and low speeds (lower than 15 km/h).

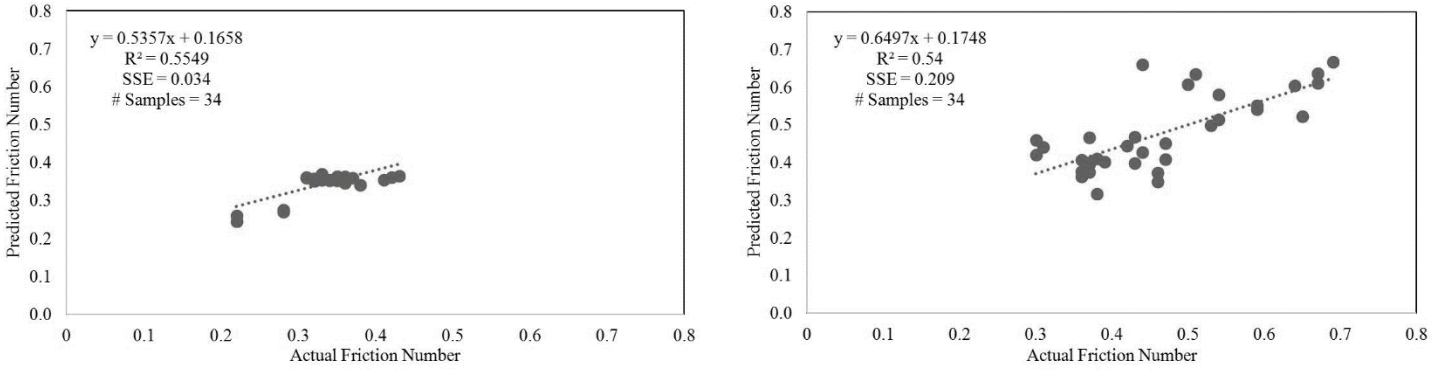

(a) Proposed Model (60 km/h)

(b) Proposed Model (10 km/h)

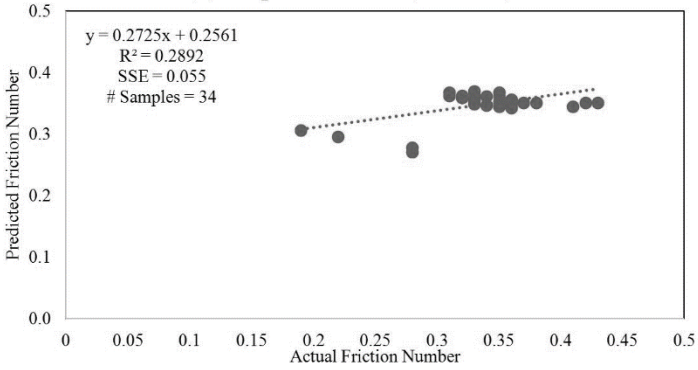

(c) Friction Model via MPD (60 km/h)

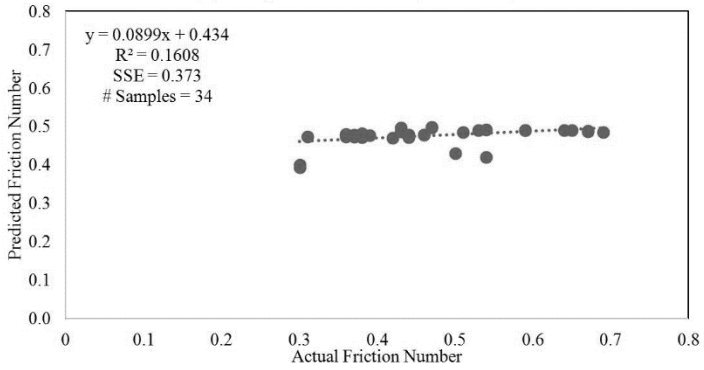

(d) Friction Model via MPD (10 km/h)

Figure 4.5 Model Validation and Comparisons

CHAPTER 5 CONCLUSIONS AND RECOMMENDATIONS

5.1 Conclusions

Five years of field data collection were performed to monitor and evaluate the long-term performance of the LTPP SPS-10 MWA site in Oklahoma. The SPS-10 site includes six sections: Sections 1 to 3 are the required SPS-10 experimental designs, while Sections 4 to 6 are the supplemental sections with mixes chosen by the ODOT Division Office. Foaming process and chemical additive produced WMA were considered in the experimental design along with binder and gradation changes.

The surface characteristics data collected include pavement cracking, rutting, roughness, macrotexture and friction. One data collection was conducted before the construction, while ten data collection events were performed after the construction, respectively in November 2015 (right after the construction), March 2016, May 2016, September 2016, January 2017, July 2017, October 2017, July 2018, March 2019, and June 2019. The newly developed 1mm PaveVision3D system, the AMES® high speed profiler and the Grip Tester were employed for the data collection at highway posted speed without interfering traffic flow. Based on the results of this study, the following conclusions can be drawn:

- The existing pavement condition before the construction did not show an influence on after-construction performance in terms of pavement

cracking, rutting, roughness, and macrotexture for both WMA and HMA sections.

- WMA Sections 2 and 3, with the same binder grade, content, and gradation as that of the HMA control section (Section 1), achieved comparable performance relative to the conventional HMA in terms of pavement cracking, rutting, roughness, macrotexture, and friction.
- WMA Section 4 showed much more transverse cracking than the HMA control section because it used PG 64-22 as its binder, one grade higher in the low temperature as compared to PG 70-28 on Section 1. However, WMA Section 4 reached similar performance to that of the control HMA section after 4 years of service in terms of rutting, roughness, macrotexture, and friction.
- No cracking was observed on WMA Section 5. For other surface characteristics, WMA Section 5 achieved comparable performance as that of the HMA control section.
- WMA Section 6 had a higher binder content (6.6%) and exhibited no cracking in June 2019. No difference was observed between WMA Section 6 and the HMA control section regarding rutting and roughness. However, Section 6 with SMA design had larger MPD values and was able to maintain higher pavement skid resistance with increasing water film depth.

In addition, to identify suitable pavement texture parameters under 3D to characterize pavement surface texture and friction performance, the LS-40 Portable

3D Surface Analyzer and the Dynamic Friction Tester were used to collect pavement texture and friction data in November 2015 (immediately after the construction of the testing site) and May 2016. Twenty-four 3D areal texture parameters from five categories, including height parameter, volume parameters, hybrid parameters, spatial parameters and feature parameters, were explored and calculated for each 3D texture data. After correlation analysis, V_{mc} (a volume parameter) and S_{pd} (a feature parameter) were identified to relate the pavement texture at macro- and micro-level for friction in wet conditions at high and low speeds, respectively. Friction prediction models with fair accuracy were developed based on the selected 3D areal texture parameters at different speeds. The selected 3D texture parameters provide better alternative to characterize texture attributes with respect to pavement friction performance.

5.2 Recommendations

Large-scale evaluation of long-term pavement performance started in the late 1980s by FHWA through the original Strategic Highway Research Program (SHRP), and later on the Long-Term Pavement Performance (LTPP) program till today. This three-decade long engineering effort has provided the pavement community valuable data and information in a systematic manner for better pavement materials, design, and management. This ODOT SPR project (2115) was launched in 2015 to specifically evaluate WMA applications that were applied to six LTPP sites in Oklahoma, designated as Specific Pavement Study (SPS) sections in the national LTPP program. Even though useful information was obtained for ODOT in the five-

year evaluation period using the innovative technologies of 3D imaging, it is recommended that this localized LTPP program be extended to another five years with the following justifications.

Pavement performance should be monitored in a true long-term manner, as evidenced in the national LTPP program and also the findings from this project. The data and their subsequent analysis in the first five-year time-series for this ODOT SPR project gave pavement engineers abundant information on the initial performance of WMA on the six SPS sites. Generally speaking, the expected lifespan of thin overlays is between 10 to 15 years before major rehabilitations are considered. Most sections in this study have minor or not had any cracks during the first five-year period. Even for Section 4, the worst performer of the sites, only transverse cracking was observed but with an increasing deterioration trend. Therefore, continuing monitoring of the six sites in the next five years will provide a more complete picture of the first 10-year's performance. Even though the advantages of WMA are clear to ODOT, the justifications of continuing the WMA practice on larger scale in the state will depend on clear evidence that superior performance in the intermediate to long terms (10-year) is confirmed.

In addition, the average RAP content in asphalt mixtures has increased from 15.6% in 2009 to 20.1% in 2017 in the U.S. (Williams et al., 2018). The FHWA is currently conducting a full-scale experiment to evaluate the fatigue cracking performance of WMA with high content RAP (0%, 20%, and 40%) and RAS (20%). However, the LTPP SPS-10 sites in Yukon, OK only contains 12% RAP and 3% RAS. Section 6 in the current SPS-10 site is WMA based SMA without any RAP and

RAS. It is thus also recommended that ODOT construct pilot WMA pavements with higher RAP and RAS contents per the national trend, and evaluate WMA's field performance to further validate their benefits, if any, in the reduction of construction cost and enhancement of sustainability.

The OSU team is to conclude in 2020 a multiyear data collection cycle on over 20 High Friction Surface Treatment (HFST) sites in multiple states through the FHWA sponsored project, Long Term Performance Monitoring of High Friction Surfacing Treatment (HFST) Sites. In this project, the OSU team collected two rounds of data each year from 2016 to 2019 on the sites using 3D laser imaging, and several other texture and friction-based devices. This evaluation project is part of FHWA Every-Day Count initiative (EDC) designed to identify and deploy innovation aimed at reducing the time it takes to deliver highway projects, enhance safety, and protect the environment. The project targeted at evaluation of surface treatment aimed to improve high-risk sections of highways for better safety.

Furthermore, the OSU team recently successfully upgraded its 3D laser imaging technology to 0.5mm resolution. This unprecedented specification would allow the 3D laser imaging technology to conduct data collection at highway speed without traffic control for fine distresses and macro-texture. The OSU team has developed tremendous amount of experience in terms of applying the most advanced 3D laser imaging technologies to monitor pavements across the nation for both performance and safety analysis.

In summary, a new five-year SPR project for the first 10-year continuous monitoring is recommended to ODOT with the following objectives:

- Continue monitoring the ODOT SPS-10 WMA pavement sites on SH66 with the new 0.5mm 3D technology to (1) perform data collection and evaluation of pavement surface characteristics and performance (including cracking, rutting, roughness, texture, friction, and hydroplaning), and (2) understand the intermediate-term and long-term performance of WMA.
- Expand the scope of the new project to include data collection and analysis on ODOT pavement sections that have friction and safety related implications in the recommended second five-year period.
- Construct additional WMA sites with high RAP and RAS contents, monitor their field performance, conduct life cycle cost analysis, and develop recommendations and guidelines for ODOT's wide adoption of WMA.

REFERENCES

AASTHO. (2013a). *Quantifying Cracks in Asphalt Pavement Surfaces from Collected Images Utilizing Automated Methods*. AASHTO Designation PP67-10. Washington, D.C.

AASTHO. (2013b). *Standard Practice for Determining Pavement Deformation Parameters and Cross Slope from Collected Transverse Profiles*. AASHTO Designation: PP69-10. American Association of State Highway and Transportation Officials. Washington, D.C.

Adelle W. (2006). Quantitative Characterisation of Surface Finishes on Stainless Steel Sheet using 3D Surface Topography Analysis. Doctoral thesis, University of Huddersfield. Huddersfield, England.

Arhin, S.A., Noel, E.C., and Ribbiso, A. (2015). Acceptable International Roughness Index Thresholds based on Present Serviceability Rating. *Journal of Civil Engineering Research*, 5(4), pp. 90-96, doi:10.5923/j.jce.20150504.03.

ASTM Designation D6433-18. (2018). *Standard Practice for Roads and Parking Lots Pavement Condition Index Surveys*. ASTM International. West Conshohocken, PA, DOI: 10.1520/ D6433-18.

ASTM Standard E1845-15. (2015). *Standard Practice for Calculating Pavement Macrotexture Mean Profile Depth*. ASTM International. West Conshohocken, PA, DOI: 10.1520/E1845-15.

ASTM Standard E1911-09a. (2009). *Standard Test Method for Measuring Paved Surface Frictional Properties Using the Dynamic Friction Tester*. ASTM International, West Conshohocken, PA, DOI: 10.1520/E1911-09AE01.

ASTM Standard E2157-15. (2015). *Standard Test Method for Measuring Pavement Macrotexture Properties Using the Circular Track Meter*. ASTM International, West Conshohocken, PA, DOI: 10.1520/E2157-15.

ASTM Standard E274/E274M-115. (2015). *Standard Test Method for Skid Resistance of Paved Surfaces Using a Full-Scale Tire*. ASTM International, West Conshohocken, PA, DOI: 10.1520/E0274_E0274M-15.

ASTM Standard E303-93. (2013). *Standard Test Method for Measuring Surface Friction Properties Using the British Pendulum Tester*. ASTM International, West Conshohocken, PA, DOI: 10.1520/E0303-93R13.

ASTM Standard E950-98. (1998). *Measuring Test Method for Measuring the Longitudinal Profile of Traveled Surfaces with an Accelerometer Established Inertial Profiling Referenc*e. ASTM International, West Conshohocken, PA.

ASTM Standard E965-15. (2015). *Standard Test Method for Measuring Pavement Macrotexture Using a Volumetric Technique*. ASTM International, West Conshohocken, PA, DOI: 10.1520/E0965-15.

Bitelli G. et al. (2012). Laser Scanning on Road Pavements: A New Approach for Characterizing Surface Texture. *Sensors*, Vol. 12, pp. 9110-9128, DOI: 10.3390/s120709110.

Bonaquist, R. (2011). *Mix Design Practices for Warm Mix Asphalt*. NCHRP Report 691, Transportation Research Board, National Research Council, Washington, D.C.

Bower N. et al. (2012). Evaluation of the Performance of Warm Mix Asphalt in Washington State. Washington DOT. Olympia, WA.

Button J.W., Estakhri C. and Wimsatt A., (2007). *A Synthesis of Warm-Mix Asphalt*. Publication FHWA/TX-07/0-5597-1. Texas Department of Transportation. Austin TX.

Cerezo, V., Do, M., Prevost, D., and Bouteldja, M. (2014). Friction/Water Depth Relationship-In Situ Observations and Its Integration in Tire/Road Friction Models. *Journal of Engineering Tribology*, 228(11), pp. 1285-1297.

Copeland, A. et al. (2010). Field Evaluation of High Reclaimed Asphalt Pavement/Warm Mix Asphalt Project in Florida: A Case Study. *Transportation Research Board Annual Meeting* CD-ROM. Transportation Research Board of the National Academies. Washington, D.C.

Dave, E.V., Hanson, C.E., Helmer, B., Dailey, J., and Hoplin, C.M. (2015). *Laboratory Performance Test for Asphalt Concrete*. Publication MN/RC 2015-24, Minnesota Department of Transportation, St. Paul, Minnesota.

D'Angelo J. et al. (2008). *Warm-Mix Asphalt: European Practice*. Publication FHWA-PL-08-007. Federal Highway Administration. Washington D.C.

Deltombe, R., Kubiak, K.J., Bigerelle, M. (2011). How to Select the Most Relevant 3D Roughness Parameters of a Surface. *Scanning*, Vol. 36, No. 1, pp. 150-160, DOI: 10.1002/sca.21113.

Diefenderfer, S. and A. Hearon. (2008). *Laboratory Evaluation of a Warm Asphalt Technology for Use in Virginia*. Publication VTRC 09-R11, Virginia Transportation Research Council, Charlottesville, VA.

Do, M. et al. (2007). Pavement Polishing-Development of a Dedicated Laboratory Test and its Correlation with Road Results. *Wear*, Vol. 263, pp. 36-42.

Do, M., Cerezo, V., Beautru, Y., and Kane, M. (2014) Influence of Thin Water Film on Skid Resistance. *Journal of Traffic and Transportation Engineering*, 2(1), pp. 36-44.

Dunford A.M. et al. (2012). Three-Dimensional Characterization of Surface Texture for Road Stones Undergoing Simulated Traffic Wear. *Wear*, Vol. 292-293, pp. 188-196.

Ergun, M., Iyinam, S., and Iyinam, A. (2005). Prediction of Road Surface Friction Coefficient Using Only Macro- and Microtexture Measurements. *Journal of Transportation Engineering*, Vol. 131, No. 4, pp. 311-319.

Flintsch G.W. et al. (2012). *The Little Book of Tire Pavement Friction*. Pavement Surface Properties Consortium. Virginia Polytechnic Institute and State University. Blacksburg, VA.

Hall J.W. et al. (2009). NCHRP *Web Document 108: Guide for Pavement Friction*. Transportation Research Board, National Research Council, Washington, D.C.

Henry, J.J. (2000). NCHRP Synthesis 291: *Evaluation of Pavement Friction Characteristics*. Transportation Research Board, National Research Council, Washington, D.C.

Hartikainen L., Petry F. and Westermann S. (2014). Frequency-wise Correlation of the Power Spectral Density of Asphalt Surface Roughness and Tire Wet Friction. *Wear*, Vol. 317, pp. 111-119.

Hurley, G. C. et al. (2006). Evaluation of potential processes for use in Warm Mix Asphalt. *Journal of the Association of Asphalt Paving Technologists*, Savannah, GA, United States, pp: 41-90.

Izeppi E., Flintsch G. and McGhee K. (2010). *Field Performance of High Friction Surfaces*. Publication FHWA/VTRC 10-CR6. Federal Highway Adminstration (FHWA). Washington, D.C.

Kanafi M.M. et al. (2015). Macro- and Micro-Texture Evolution of Road Pavements and Correlation with Friction. *International Journal of Pavement Engineering*, Vol. 16, No. 2, pp. 168-179, DOI: 10.1080/10298436.2014.937715.

Kane M., Rado Z. and Timmons A. (2015). Exploring the Texture-Friction Relationship: from Texture Empirical Decomposition to Pavement Friction.

International Journal of Pavement Engineering, Vol. 16, No. 10, pp.919-918, DOI:10.1080/10298436.2014.972956.

Kvasnak, A., J. Moore, A. Taylor, and B. Prowell. (2010). *Evaluation of Warm Mix Asphalt Field Demonstration: Nashville, Tennessee*. NCAT Report 10-01, National Center for Asphalt Technology. Auburn, AL.

Leach R. (2012). *Characterisation of Areal Surface Texture*. Springer-Verlag Berlin Heidelberg, Berlin Germany. DOI: 10.1007/978-3-642-36458-7.

Lin Li, Kelvin. C.P. Wang, and Qiang Li (2016). Geometric Texture Indicators for Safety on AC Pavements with 1 mm 3D Laser Texture Data. *International Journal of Pavement Research and Technology*, Vol. 9, pp. 49-62.

Li Shuo, Samy Noureldin, Karen Zhu, and Yi Jiang (2016). Pavement Surface Microtexture: Testing, Characterization and Frictional Interpretation. *STP 1555, Pavement Performance: Current Trends, Advances, and Challenges*. West Conshohocken, PA.

Liu Q. and Shalaby A. (2015). Relating Concrete Pavement Noise and Friction to Three-Dimensional Texture Parameters. *International Journal of Pavement Engineering*, Volume 18 (5), pp. 450-458. DOI: 10.1080/10298436.2015.1095897.

Michigan Metrology. (2014). *Michigan Metrology Surface Texture Parameters Glossary*. Michigan Metrology, Lansing, MI.

Mohammad, L., Hassan, M., Vallabhu, B., and Kabir, M. (2015). Louisiana's Experience with WMA Technologies: Mechanistic, Environmental, and Economic Analysis. *Journal of Materials in Civil Engineering*, 27(6): 04014185.

Nataadmadja A.D. et al. (2012). Quantifying Aggregate Microtexture with Respect to Wear-Case of New Zealand Aggregates. *Wear*, Vol. 332-333, pp. 907-917.

National Asphalt Pavement Association (NAPA). (2002). *Designing and Constructing SMA Mixtures—State-of-the-Practice*. Quality Improvement Series 122, NAPA, Lanham, Maryland.

Prowell, B. D., G. C. Hurley, and E. Crews. (2007). Field Performance of Warm Mix Asphalt at the NCAT Test Track. *Transportation Research Board Annual Meeting* CD-ROM, Transportation Research Board of the National Academies, Washington, D.C.

West, R., et al. (2014). *Field Performance of Warm Mix Asphalt Technologies*. NCHRP REPORT 779. Transportation Research Board of the National Academies, Washington, D.C.

Sargand, S., Nazzal, M.D., AI-Rawashdeh, A., and Powers, D. (2012). Field Evaluation of Warm-Mix Asphalt Technologies. *Journal of Materials in Civil Engineering*, 24(11), pp. 1343-1349. DOI: 10.1061/(ASCE)MT.1943-5533.0000434.

Serigos P.A. (2013). The Contribution of Micro- and Macro-Texture to the Skid Resistance of Pavements. http://www.ectri.org/YRS13/Documents/Presentations/Session5b-6a/YRS13_Session5b-6a_Serigos_TRB.pdf. Accessed 12 May, 2016.

Ueckermann et al. (2015). A Contribution to Non-contact Skid Resistance Measurement. *International Journal of Pavement Engineering*, Vol. 16, No. 7, pp. 646-659, DOI:10.1080/10298436.2014.943216.

Villani M.M. et al. (2014). Application of Fractal Analysis for Measuring the Effects of Rubber Polishing on the Friction of Asphalt Concrete Mixtures. *Wear*, Vol. 320, pp. 179-188.

Wang, K.C.P. et al. (2015). Network Level Pavement Evaluation with 1 mm 3D Survey System. *Journal of Transportation Engineering*, 2(6), pp. 391–398.

West, R. et al. (2011). *Field Performance of Warm Mix Asphalt Technologies*. NCHRP Report 779, Transportation Research Board, National Research Council, Washington, D.C.

Wielinski, J., A. Hand, and D. M. Rausch. (2009). Laboratory and Field Evaluations of Foamed Warm Mix Asphalt Projects. *Transportation Research Record*, No. 2126, pp. 125-131. Transportation Research Board, National Research Council, Washington, D.C.

Williams, Brett A., Audrey Copeland, and T. Carter Ross (2018). *Asphalt Pavement Industry Survey on Recycled Materials and Warm-Mix Asphalt Usage*. 2017. Information Series 138 (8th edition). National Asphalt Pavement Association. Lanham, MD.

Yang, G. et al. (2018). Wavelet based macrotexture analysis for pavement friction prediction. *KSCE Journal of Civil Engineering*, Vol. 22(1), pp. 117–124. https://doi.org/10.1007/s12205-017-1165-x.

Zelelew H.M. et al. (2014). Wavelet-based Characterisation of Asphalt Pavement Surface Macro-texture. *Road Materials and Pavement Design*, Vol. 15, No. 3, pp. 622-641, DOI:10.1080/14680629.2014.908137.

Zhang, A. et al. (2017). Automated Pixel-Level Pavement Crack Detection on 3D Asphalt Surfaces Using a Deep-Learning Network. *Computer-Aided Civil and Infrastructure Engineering*, Vol. 32, pp. 805–819.

Zhang, A. et al. (2018). Pavement Lane Marking Detection Using Matched Filter. *Measurement*, Vol. 130, pp. 105-117.